# AGES: The AGN and Galaxy Evolution Survey<sup>1</sup>

C.S. Kochanek<sup>1,2</sup>, D.J. Eisenstein<sup>3</sup>, R.J. Cool<sup>4</sup>, N. Caldwell<sup>3</sup>, R.J. Assef<sup>5</sup>, B.T. Jannuzi<sup>6</sup>, C. Jones<sup>3</sup>, S.S. Murray<sup>3,7</sup>, W.R. Forman<sup>3</sup>, A. Dey<sup>6</sup>, M.J.I. Brown<sup>8</sup>, P. Eisenhardt<sup>5</sup>, A.H. Gonzalez<sup>9</sup> P. Green<sup>3</sup>, D. Stern<sup>5</sup>

## ABSTRACT

The AGN and Galaxy Evolution Survey (AGES) is a redshift survey covering, in its standard fields, 7.7 deg<sup>2</sup> of the Boötes field of the NOAO Deep Wide-Field Survey (NDWFS). The final sample consists of 23745 redshifts. There are well-defined galaxy samples in ten bands (the  $B_W$ , R, I, J, K, IRAC 3.6, 4.5, 5.8 and 8.0 $\mu$ m and MIPS 24 $\mu$ m bands) to a limiting magnitude of I < 20 mag for spectroscopy. For these galaxies, we obtained 18163 redshifts from a sample of 35200 galaxies, where random sparse sampling was used to define statistically complete sub-samples in all ten photometric bands. The median galaxy redshift is 0.31, and 90% of the redshifts are in the range 0.085 < z < 0.66. AGN were selected as radio, X-ray, IRAC mid-IR and MIPS 24 $\mu$ m sources to fainter limiting magnitudes (I < 22.5 mag for point sources). Redshifts were obtained for 4764 quasars and galaxies with AGN signatures, with 2926, 1718, 605, 119 and 13 above redshifts of 0.5, 1, 2, 3 and 4, respectively. We detail all the AGES selection procedures and present the complete spectroscopic redshift catalogs, spectra, and spectral energy distribution decompositions. Photometric redshift estimates are for all sources in the AGES samples.

Subject headings: surveys; galaxies; quasars

<sup>&</sup>lt;sup>1</sup>Department of Astronomy, Ohio State University, 140 West 18th Avenue, Columbus, OH 43210

<sup>&</sup>lt;sup>2</sup>Center for Cosmology and Astroparticle Physics, Ohio State University, 191 W. Woodruff Avenue, Columbus, OH 43210

<sup>&</sup>lt;sup>3</sup>Harvard-Smithsonian Center for Astrophysics, 60 Garden Street, Cambridge MA 02138

<sup>&</sup>lt;sup>4</sup>Hubble and Carnegie/Princeton Fellow, Department of Astrophysical Sciences, Princeton University, Peyton Hall, Princeton NJ 08544 and The Observatories of the Carnegie Institution of Washington, 813 Santa Barbara Street, Pasadena, CA 91101

<sup>&</sup>lt;sup>5</sup> Jet Propulsion Laboratory, California Institute of Technology, 4800 Oak Grove Drive, Pasadena, CA 91109

<sup>&</sup>lt;sup>6</sup>NOAO, 950 North Cherry Avenue, Tucson, AZ, 85719

<sup>&</sup>lt;sup>7</sup>Department of Physics and Astronomy, Johns Hopkins University, Baltimore, MD, 21218

<sup>&</sup>lt;sup>8</sup>School of Physics, Monash University, Clayton, Victoria 3800, Australia

<sup>&</sup>lt;sup>9</sup>Department of Astronomy, Bryant Space Science Center, University of Florida, Gainesville, FL 32611, USA

<sup>&</sup>lt;sup>1</sup>Observations reported here were obtained at the MMT Observatory, a joint facility of the Smithsonian Institution and the University of Arizona.

### 1. Introduction

Surveys are a critical tool for understanding the evolution of galaxies and AGN. Because their properties are diverse and changing, we utilize large statistical samples of galaxies to measure the distribution of their properties and to trace the evolution of these distributions. Achieving a suitably high level of detail requires a combination of multiwavelength imaging and spectroscopy. Without a redshift estimate, one cannot infer luminosity, color, or environmental density, all quantities known to be of central importance in the behavior of galaxies and AGN. While photometric redshifts can be used in the absence of spectroscopy, they have more systematic uncertainties (e.g. Hildebrandt et al. 2010) and have difficulty with AGN (e.g. Brodwin et al. 2006, Rowan-Robinson et al. 2008, Assef et al. 2010). Moreover, the story of galaxy evolution involves many wavelengths of light: UV and far-IR for young stars, optical and near-IR for older stars, and X-ray, radio and mid-IR for nuclear activity.

Decades of surveys have quantified the luminosity, color, surface brightness, star formation, and nuclear activity of low redshift galaxies and correlated these properties with environment. The combination of the CfA Redshift Survey (de Lapparent et al. 1986) and the Palomar Sky Survey (POSS-II, Reid et al. 1991) defined the state of the art for local galaxies in the 1980's. This was followed by the Las Campanas Redshift Survey and its drift-scan CCD imaging (Shectman et al. 1996), which expanded our view to larger scales. Most recently, the 2 Degree Field Galaxy Redshift Survey (Colless et al. 2001) and the Sloan Digital Sky Survey (SDSS York et al. 2000) brought the scale of spectroscopy to the million-galaxy level. Wide area digital imaging from the 2 Micron All-Sky Survey (2MASS, Skrutskie et al. 2006), SDSS, GALEX (Martin et al. 2005), the Spitzer Space Telescope (Werner et al. 2004), and ROSAT (e.g. Voges et al. 1999) have been combined with this spectroscopy to build a detailed characterization of nearby galaxies.

Surveys at higher redshift require much deeper imaging and fainter spectroscopy. Projects such as GOODS (Giavalisco et al. 2004), DEEP-2 (e.g. Faber et al. 2007), VVDS (Le Fèvre et al. 2005), and COSMOS (Scoville et al. 2007) now aim to survey cosmologically interesting volumes at redshifts of order unity and above. Importantly, there is substantial evolution in galaxy properties. Since  $z\approx 1$ , the star formation rate per unit comoving volume has dropped by a factor of 10 (e.g. Hopkins & Beacom 2006), the frequency of luminous quasars (e.g. Croom et al. 2004, Richards et al. 2005, Richards et al. 2006) and ultra-luminous infrared galaxies have decreased by a factor of 100 (e.g. Cowie et al. 2004, Le Floc'h et al. 2005), the mass of galaxies on the red sequence has roughly doubled (e.g. Bell et al. 2003, Faber et al. 2007), and the typical site for star formation has moved to less massive galaxies (e.g. Cowie et al. 1996). At redshifts above unity, further evolution is clear, with galaxies getting notably smaller (e.g. Daddi et al. 2005, van Dokkum et al. 2010), possibly with changing correlations of star formation with environment (e.g. Scodeggio et al. 2009, Cooper et al. 2010).

Mapping galaxy properties at intermediate redshift ( $z \sim 0.5$ ) and the demographics of active galactic nuclei (AGN) at any redshift requires wider fields than these deep surveys can provide.

We designed the AGN and Galaxy Evolution Survey (AGES) to address these questions, combining spectroscopy from the Hectospec instrument on the MMT (Fabricant et al. 1998, Roll et al. 1998, Fabricant et al. 2005) with superb multi-wavelength imaging in the NOAO Deep Wide-Field Survey (NDWFS) Boötes field. This field contains deep imaging at optical and near-IR bands (Jannuzi & Dey 1999, Elston et al. 2006) as well as full-field coverage from Spitzer IRAC (Eisenhardt et al. 2004 and later Ashby et al. 2009) and MIPS (Soifer & Spitzer/NOAO Team 2004), Chandra (Murray et al. 2005, Kenter et al. 2005, Brand et al. 2006), GALEX (Martin et al. 2005), and radio (Becker et al. 1995, de Vries et al. 2002) facilities. As we detail below, AGES provides spectroscopic redshifts for 18163 galaxies to I = 20 and 4764 AGN to I = 22.5 in the 9 square degree field.

AGES sought to exploit the diversity of available imaging data by a multi-faceted targeting strategy. AGN were selected by optical color, IRAC color, and MIPS, X-ray, or radio detection. The result is a large and broad sample of AGN, including nearly 200 per square degree at z>1 and nearly 400 per square degree in total. The galaxy sample required sparse sampling to reach I=20, but we tuned the sparse sampling algorithm to ensure full sampling of brighter magnitude thresholds in ten different bands from the UV to the mid-IR. The AGES observational strategy returned to the field many times with rolling acceptance, with the result of very high completeness in the statistical samples. This also means that fiber collisions are an unimportant problem even in high density regions. AGES is well tuned for the study of galaxy properties at 0.2 < z < 0.6 and AGN properties out to z=5 over a cosmologically sized volume with pan-chromatic spectral energy distributions.

This paper presents the AGES data set and data release. Section 2 describes survey design and target selection. Section 3 discusses the observations themselves. Section 4 describes the data reduction procedures. Section 5 summarizes the resulting samples and Section 6 introduces the files of the data release. We conclude in Section 7. All magnitudes and fluxes are in the system used by the parent survey. These are Vega magnitudes for the  $B_w$ , R, I, J, K,  $K_s$  and IRAC bands, AB magnitudes for the FUV, NUV and z' bands, mJy for MIPS  $24\mu$ m band and the radio observations, and 0.5-7 keV counts for the X-ray observations.

# 2. Survey Design

We selected targets at all wavelengths from radio through X-ray to take full advantage of the available imaging data. We start with the optical data of the NDWFS itself in the  $B_W$ , R and I bands (Jannuzi & Dey 1999), since our ability to measure spectra is limited by the optical flux. We used the zBoötes (Cool 2007) data to help target high-redshift quasars. In the near-infrared we used the K-band data of the NDWFS and the J/K<sub>s</sub>-band data of the FLAMEX survey (Elston et al. 2006). In the mid-infrared we used the 3.6, 4.5, 5.8 and 8.0 $\mu$ m data from the IRAC Shallow Survey (Eisenhardt et al. 2004). We used the 24 $\mu$ m data from Soifer & Spitzer/NOAO Team (2004). In the radio we used the FIRST survey (Becker et al. 1995) and the deeper 1.4 GHz WSRT catalog of

de Vries et al. (2002). Going to shorter wavelengths we used data from GALEX (Martin et al. 2005) in the UV and the Chandra XBoötes survey (Murray et al. 2005, Kenter et al. 2005, Brand et al. 2006) at X-ray wavelengths.

Our general approach was to produce well-defined, magnitude limited samples of galaxies at all the available wavelengths from  $24\mu\mathrm{m}$  through the GALEX FUV bands, and to target AGN using a broad range of selection methods to a somewhat deeper optical flux limit. The galaxy samples were generally designed to be complete to an intermediate magnitude limit and then randomly sparse sampled from this intermediate limit to the overall magnitude limit. The sample definitions changed several times, with the largest change being a shift from preliminary photometric catalogs and R-band magnitude limits to revised catalogs and I-band magnitude limits between the 2004 and 2005 observing seasons.

Sparse sampling was an essential component of our strategy for studying galaxies because it was the only means of covering such a wide area to the desired depth (I < 20 mag) in reasonable time. To begin with, sparse sampling over a wider area produces samples with less cosmic variance than complete samples in smaller areas surveying smaller cosmological volumes. It also allows us to sample galaxies with very different properties with a well-defined statistical approach. In particular, by making the survey complete for bright objects and sparse sampling across many different photometric bands for fainter objects, we have a final sample with less shot noise for bright objects and the relatively rarer objects with extreme colors in any band. While the approach is more complex than previous redshift surveys, it is nonetheless straight forward to construct a complete statistical sample by weighting each object by the inverse of its sampling fraction We provide explicit instructions on the appropriate procedures in  $\S 6$ .

In §2.1, 2.2 and 2.3 we define nomenclature, outline our approach to random sparse sampling, and define the standard AGES sub-fields. In §2.4, 2.5, and 2.6 we outline the sample definitions used in 2004, 2005 and 2006/2007. Samples defined in the previous years continued to be observed at the same priorities in the later years. The biggest differences were between 2004 and the later years, where we (1) shifted from an R-band limited sample in 2004 to an I-band limited sample, (2) shifted from preliminary NDWFS and IRAC Shallow Survey catalogs to later versions, and (3) added mid-IR quasar selection. The main differences from 2005 to 2006/2007 were to add sub-samples further exploring mid-IR quasar selection and to include the zBoötes data as a tool for AGN selection. There are many other small differences that are detailed in each subsection. We provide the selection codes for all seasons, so that it is clear why any source may have been targeted, but in the data tables we only provide the photometric information for the updated catalogs used from 2005 onwards. The photometric data are only a limited representation of the underlying catalogs – the original survey catalogs should be consulted to obtain the complete data. In each season we targeted at low priority some objects that were not part of the primary AGES project as experiments from collaborators We very briefly outline these experiments and include their selection codes but provide no details.

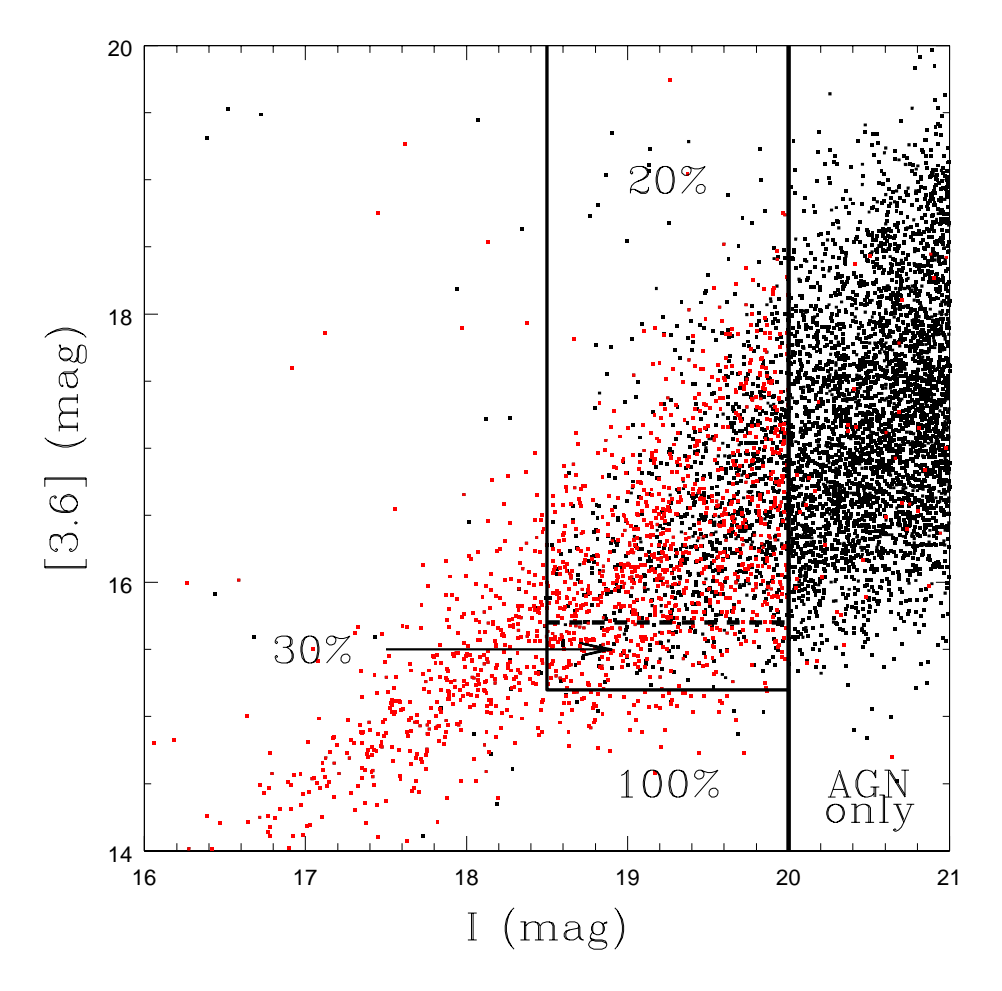


Fig. 1.— The distribution of galaxies in I band and IRAC [3.6] magnitudes. The points are a randomly selected 10% of the sources in the main survey area, where red points have measured redshifts. The boundaries indicate the survey sampling regions and the sparse sampling rates. The actual fractions of redshift measurements in these regions are much higher than the nominal 20% or 30% sampling rates because of the different color weightings of the various bands and the observations of lower priority sources with unused fibers. AGN were targeted to fainter magnitudes, leading to the redshift measurements with I > 20 mag.

#### 2.1. Common Definitions

We will refer to the survey bands as X, FUV, NUV,  $B_W$ , R, I, z, J, K,  $[3.6]_i$ ,  $[4.5]_i$ ,  $[5.8]_i$ ,  $[8.0]_i$ , [24], FIRST, and WSRT. For the X-ray sources, X is the X-ray counts from the XBoötes survey. For the ultraviolet sources, FUV and NUV are the two GALEX filters. For the optical and near-IR,  $B_W$ , R, I, z', J and K are the SExtractor Kron-like (mag\_auto) magnitudes. The K refers to both the NDWFS K/K<sub>s</sub> and the FLAMEX K<sub>s</sub> data. The final NDWFS magnitudes are from DR3 (http://www.noao.edu/noao/noaodeep/DR3/dr3-data.html). For the IRAC data,  $[3.6]_i$ – $[8.0]_i$  are the 3.6, 4.5, 5.8 and 8.0 $\mu$ m SExtractor Kron-like magnitudes where the subscript i = [3.6]–[8.0] defines the IRAC band used to define the extraction apertures. The 24 $\mu$ m flux [24] is the DAOPHOT PSF-fit flux of the source. FIRST and WSRT both measured 1.4 GHz radio continuum fluxes. Where we are using the flux in a fixed aperture, we add the aperture diameter to the magnitude, so  $[3.6]_{[3.6]}(6''.0)$  represents the IRAC 3.6 $\mu$ m flux in a 6''.0 diameter aperture whose position was determined from the 3.6 $\mu$ m image. These IRAC aperture magnitudes are, however, corrected for the extension of the IRAC point spread function beyond the aperture.

For the optical data we homogenized several aperture magnitudes for seeing variations. For each field, we took stars in the magnitude range 19 < I < 20 and computed the mean differences between the Kron-like I magnitude, presumed to be seeing independent, and the 1".0, 3".0 and 6".0 aperture magnitudes. These differences, which show the expected pattern of being significant for the 1".0 apertures and negligible of the 6".0 apertures, were then applied to these three aperture magnitudes for the  $B_W$ , R and I bands.

Point sources (pntsrc = 1) were defined based on the SExtractor stellarity indices of the sources in the optical ( $B_W$ , R, I and z'-bands). For each target we assigned a code (bgood, rgood, igood, zgood= 1) for whether the data in each band on that target was acceptable. We flagged objects as either quasar candidates (qso = 1), galaxies (galaxy = 1), or in the later seasons AGN-galaxy (agngalaxy = 1) targets. Quasar candidates are point sources brighter than the (optical) magnitude limit for targeting quasars, galaxies are extended sources brighter than the magnitude limit for targeting galaxies, and "AGN-galaxies" are extended AGN candidates brighter than the magnitude limit for targeting quasars but fainter than that for galaxies. In general, our sources are much brighter than the NDWFS survey limits, so there are few issues with star/galaxy separation.

### 2.2. Sparse Sampling Codes

For many of our samples we observed all targets to an intermediate magnitude limit and then randomly sparse sampled the sources between the intermediate limit and the overall flux limit of the sample. All sources were assigned a random integer code  $0 \le \text{rcode} < 20$  dividing the sources into 20 random sub-samples each containing 5% of the targets. Once assigned to a source, these codes were preserved in all future samples. The sparse sampling fraction was then determined by the limit on the rcode used to define the sample. For objects that were not included in any of

the primary samples, we assigned lower rcode values higher observing priorities than higher rcode values. This increases the completeness of the observations for the lower rcode targets, so that any decision to move to a higher sparse sampling fraction than used initially requires observations of fewer targets while ensuring that the fibers stay filled.

Fig. 1 illustrates how this works for the IRAC [3.6] sample in 2006/2007 (see below). All galaxies must have I < 20 mag, so no fainter objects were targeted unless they appeared in one of the AGN samples. At I band, all galaxies were targeted if they were brighter than I < 18.5 mag, and a randomly selected 20% (rcode  $\leq$  3) were targeted between 18.5 < I < 20. For the IRAC [3.6] band, galaxies were all targeted if brighter than [3.6] < 15.2 mag, and a randomly selected 30% (rcode  $\leq$  5) were targeted between 15.2 < [3.6] < 15.7, but still subject to the I < 20 mag limit. Combining these criterion, all sources to the left or below the heavy solid line, 30% of the sources in the box 18.5 < I < 20 and 15.2 < [3.6] < 15.7, and 20% of the sources with 18.5 < I < 20 and [3.6] > 15.7 mag were targeted by these criterion. Between the different color weightings of the bands and the filling of fibers that could not be allocated to the primary samples, the actual fractions of sources with redshift measurements in the sparse sampling regions are much higher than 20% or 30%.

### 2.3. Standard Fields

We defined our primary statistical samples as the union of the NDWFS field geometry with a set of 15 sub-fields defined by the Hectospec field of view. Sources had to lie within 0.49 deg of one of the 15 field centers illustrated in Fig. 2 and listed in Table 1. The field centers were simply defined by the final field centers used for the primary observational runs in 2004. Sources inside the standard sub-fields are assigned the field ID of the closest field center, while those outside are assigned a field ID of -1 (see Table 2). Several of the circular fields extend beyond the NDWFS area, so the actual survey area must be clipped to exclude RA < 228.96 deg, Dec > 33.46 deg, and Dec < 35.84 deg if RA > 216.14 deg. The total area within this region is  $2.40 \times 10^{-3}$  sr (7.88 deg<sup>2</sup>). We also do not target sources within radius  $R_{bstar}/2$  of a bright  $R_{USNO} < 17$  mag USNO star, where  $R_{bstar} = 20''.0 + 5''.0(15 - R_{USNO})$ . For  $R_{bstar}/2 < R < R_{bstar}$ , there were additional surface brightness criteria for observing targets (see below). Excluding the bright star exclusion areas with  $R < R_{bstar}/2$ , the survey area drops to  $2.36 \times 10^{-3}$  sr (7.74 deg<sup>2</sup>).

The next three sub-sections describe the evolving selection criteria. Most readers should proceed to §2.6 which defines the final sample selection criteria. The criteria for the earlier observations in §2.4 and §2.5 are supplied for completeness and because all objects targeted in these earlier seasons continued to be targeted in the later seasons independent of any revisions to the selection criteria. Tables 3 and 4 summarize the final samples and their completeness.

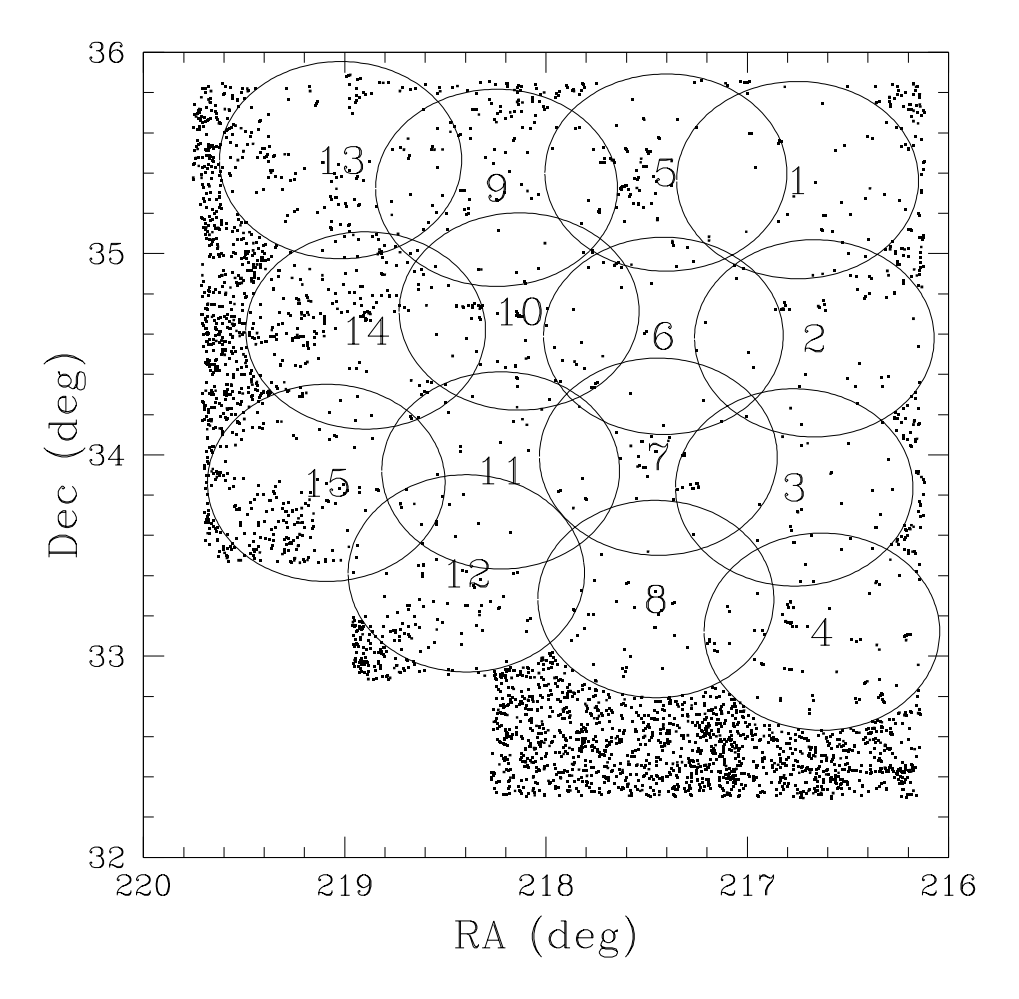


Fig. 2.— The 15 standard sub-fields listed in Table 1. The points are the 2006/2007 primary galaxy sample targets (gcode06 neither zero nor 2048) lacking redshifts. Note the high completeness in the sub-fields and the significantly lower completeness elsewhere in the Boötes field. Some redshifts were obtained outside the standard fields because of the shifting centers of the individual Hectospec pointings.

# 2.4. 2004 Sample Definitions

The 2004 samples were based on preliminary NDWFS and IRAC Shallow Survey catalogs and photometric calibrations. The observations also immediately followed the initial engineering runs for Hectospec. Since there was no experience with the performance of Hectospec in the red, we decided to set our optical selection criterion using a catalog<sup>2</sup> to an R-band magnitude limit of R < 21.5 so that K-corrections would minimize the number of galaxies with z > 0.5. The NDWFS optical photometry was flagged as good if the Kron-like, mag\_auto magnitude was defined (magnitude between 0 and 80), the SExtractor flags were FLAGS < 8, catalog duplication flag FLAG\_DUPLICATE = 0 and it was detected in more than one sub-images available for the band. A galaxy (galaxy = 1) was required to have good data in R and either I or  $B_W$ , SExtractor stellarity indices  $\leq 0.8$  in all bands, R  $\leq 20$  mag and R<sub>ap1</sub>  $\leq 23.5$  mag. Star/galaxy separation in the NDWFS catalogs based on the SExtractor stellarity indices is effective to significantly fainter fluxes than our spectroscopic flux limits. We explicitly included all galaxies found in the 2MASS survey and excluded all galaxies within radius  $20''.0 - R_{USNO}$  of a USNO star with  $R_{USNO} \leq 17$  mag. A quasar target needed to have  $17 < R \le 21$ , good R-band data, and not have galaxy = 1. There were 15 target groups defined for 2004 defined by the binary target code code04. The complete, main Rband galaxy sample is the combination of code04 = 2048 (bright R-band galaxies) and code04 = 512(20% sparse sampling of fainter R-band galaxies). After the first series of observations, we were beginning to exhaust the AGN targets, so we added the fainter X-ray and MIPS target categories as well as a set of experimental brown dwarf candidates (code04 = 4096, 8192 and 16384) at lower priority. Because these observations were significantly dependent on preliminary photometry, we include the targeting information but not the underlying photometry in this paper. The 15 samples are:

- SDSS Flux Calibration Stars (code04 = 1): These are candidate F-stars selected on the basis of SDSS photometry that are used to flux calibrate the spectra. We tried to include 5 of these flux calibration stars in each observation.
- IRAC  $8.0\mu m$  galaxy sample (code04 = 2): All galaxies (galaxy = 1) with  $[8.0]_{[3.6]}(6''.0) \le 13.2$  mag and R  $\le 20$  mag. As a reminder, all four IRAC samples were based on preliminary versions of the IRAC Shallow Survey catalogs.
- IRAC 5.8 $\mu$ m galaxy sample (code04 = 4): All galaxies with [5.8]<sub>[3.6]</sub>(6".0)  $\leq$  14.7 mag and R  $\leq$  20 mag.
- IRAC 4.5 $\mu$ m galaxy sample (code04 = 8): All galaxies with [4.5]<sub>[3.6]</sub>(6".0)  $\leq$  15.2 mag and R  $\leq$  20 mag.
- IRAC 3.6 $\mu$ m galaxy sample (code04 = 16): All galaxies with [3.6]<sub>[3.6]</sub>(6".0)  $\leq$  15.2 mag and R  $\leq$  20 mag.

 $<sup>^2</sup>$ NDWFS\_R2150\_rot\_apr08\_newcat

- MIPS  $24\mu \text{m}$  Sources (code04 = 32): These targets were galaxies or point sources with  $F_{24} \ge 1$  mJy with optical flux limits of  $R \le 20$  for galaxies and  $R \le 21.5$  for stellar targets and  $R_{ap1} < 23.5$  for both. Stellar targets also had to either lack 2MASS detections or have  $J > 12 2.5 \log(F_{24}/\text{mJy})$  mag in order to eliminate normal stars. We will illustrate this criterion for the later seasons where we used an I-band variant of this criterion.
- Blue Galaxy Sample (code04 = 64): This sample consisted of all galaxies with  $B_W < 20.5 \text{ mag}$ , bgood = 1 and  $R \le 20 \text{ mag}$ .
- Compact FIRST Sources (code04 = 128): This sample consists of FIRST radio sources with deconvolved axes smaller than 1".0 whose positions were within 3".0 of an  $R \leq 21.5$  and  $R_{ap1} \leq 23.5$  optical source. Here, and in the X-ray samples, this latter criterion was to ensure that the flux in a Hectospec fiber was large enough to plausibly measure the redshift.
- Bright X-ray Quasar Candidates (code04 = 256): This sample consists of sources from the XBoötes catalog with 4 or more X-ray counts that were matched to the R  $\leq$  21.5 optical catalog and also have  $R_{ap1} < 23.5$ , independent of whether they were extended or stellar sources.
- Main Faint R-band galaxy sample (code04 = 512): This sample consists of a randomly selected 20% (rcode  $\leq$  3) of galaxies with 19.2 < R  $\leq$  20 mag. The complete main R-band galaxy sample consists of this sub-sample plus the bright R-band galaxy sample (code04 = 2048).
- Faint R-band galaxies (code04 = 1024): This sample consists of all galaxies with  $19.2 < R \le 20$  mag. The first 20% of these galaxies (rcode  $\le 3$ ) are part of the Main Faint R-band Galaxy Sample (code04 = 512) as well, and are observed at high priority. The remaining galaxies were observed with priorities that favored lower rcodes over higher rcodes.
- Main Bright R-band galaxy sample (code04 = 2048): This sample consists of all galaxies with  $R \le 19.2$  mag.
- Fainter X-ray sources (code04 = 4096) These are fainter (2 or 3 count) sources from the XBoötes survey. Otherwise the criteria were the same as for the main X-ray sample. While targeting 2 count X-ray sources sounds odd, the backgrounds of the XBoötes survey are so low that almost all such sources associated with optical sources brighter than the spectroscopic flux limits will be real.
- Fainter MIPS point sources (code04 = 8192): These were point sources with  $0.5 \le F_{24} \le 1.0$  mJy that otherwise satisfied the point source criteria for the main MIPS sample. Galaxies were not included here.
- IRAC brown dwarf candidates (code04 = 16384): These targets were supplied by M. Ashby as an experiment, and were all found to be star forming galaxies. Since they are not part of

the primary AGES samples, we include them without further discussion because they were a low priority targeting criterion.

## 2.5. 2005 Sample Definitions

The 2005 sample definitions were very different from those in 2004 because the primary optical band was changed from the R-band to the I-band. It was clear at this point that Hectospec would work well at our desired flux levels as the 4000Å break moved beyond the R band, and we wanted the evolutionary leverage from pushing the typical redshift upwards that would be gained from using an I-band flux limit. We started with all objects having  $I \leq 21.5$  mag in the NDWFS DR3 catalogs and then matched them to all the other bands. The NDWFS optical photometry was flagged as good if the Kron-like, mag-auto magnitude was defined (magnitude between 0 and 80), the SExtractor flags were FLAGS < 8, the catalog duplication flag was FLAG\_DUPLICATE = 0 and photometric data was available (FLAG\_PHOT = 1). An object was defined as a point source (pntsrc = 1) if it had a SExtractor stellarity index  $\geq 0.8$  in any of the  $B_W$ , R, or I-bands. An object was a good target (good = 1) if igood = 1 and either bgood or rgood = 1. Galaxy targets (galaxy = 1) were good (good = 1), extended (pntsrc = 0) targets with  $I \leq 20$  mag,  $I_{ap1} \leq 24$  and  $I_{ap6} \leq 21$  mag. Quasar targets (qso = 1) were good (good = 1), point sources (pntsrc = 1) with  $I \leq 21.5$  mag and  $I_{ap1} \leq 24$ . We only attempted to obtain redshifts for galaxies and quasars with I > 15 and 16 mag respectively. The redshifts of brighter sources were filled in using SDSS (e.g. DR7, Abazajian et al. 2009). We also used the final rather than the preliminary versions of the IRAC Shallow Survey catalogs (Eisenhardt et al. 2004) and switched to using the Kron-like magnitudes  $([3.6]_{[3.6]}\cdots [8.0]_{[8.0]})$  rather than the 6"0 aperture magnitudes  $([3.6]_{[3.6]}(6".0)\cdots [8.0]_{[8.0]}(6".0))$ . Only a small portion of the NDWFS field had been observed by GALEX at this point, and the GALEX UV-selected galaxy samples based on these preliminary catalogs probably should not be directly used.

The Kron-like I-band SExtractor magnitudes clearly had significantly more problems near bright stars than the R-band magnitudes used in 2004, as shown in Fig. 3. We flagged galaxies as being potentially affected by bright stars (bstar = 1) if they lay within the magnitude dependent radius  $R_{bstar} = 20.0^{\circ} + 5.0^{\circ} (15 - R_{USNO})$  of a star with an R-band USNO magnitude  $R_{USNO} \le 17$  mag. Galaxies with bstar = 1 were rejected (galaxy = 0) if they had a surface brightness  $I_{ap6} > I + 4[(I - 20)/8]^2$  mag or they were within  $R_{bstar}/2$  of a bright star. Eqn. 1 in §6 gives a procedure from Cool et al. (2011) for controlling this problem.

There were 20 sub-samples in the 2005 survey definition. Galaxy samples were now defined at the GALEX FUV and NUV, I-band, J-band and K-band as well as the  $B_W$ , R, IRAC and MIPS bands. Quasar samples were now defined in the IRAC and optical bands in addition to the X-ray, MIPS and radio targeting, and we used the WSRT radio sources rather than FIRST. Since the full code05 values were becoming unwieldy, we also assigned sub-codes for galaxy (gcode05) and quasar

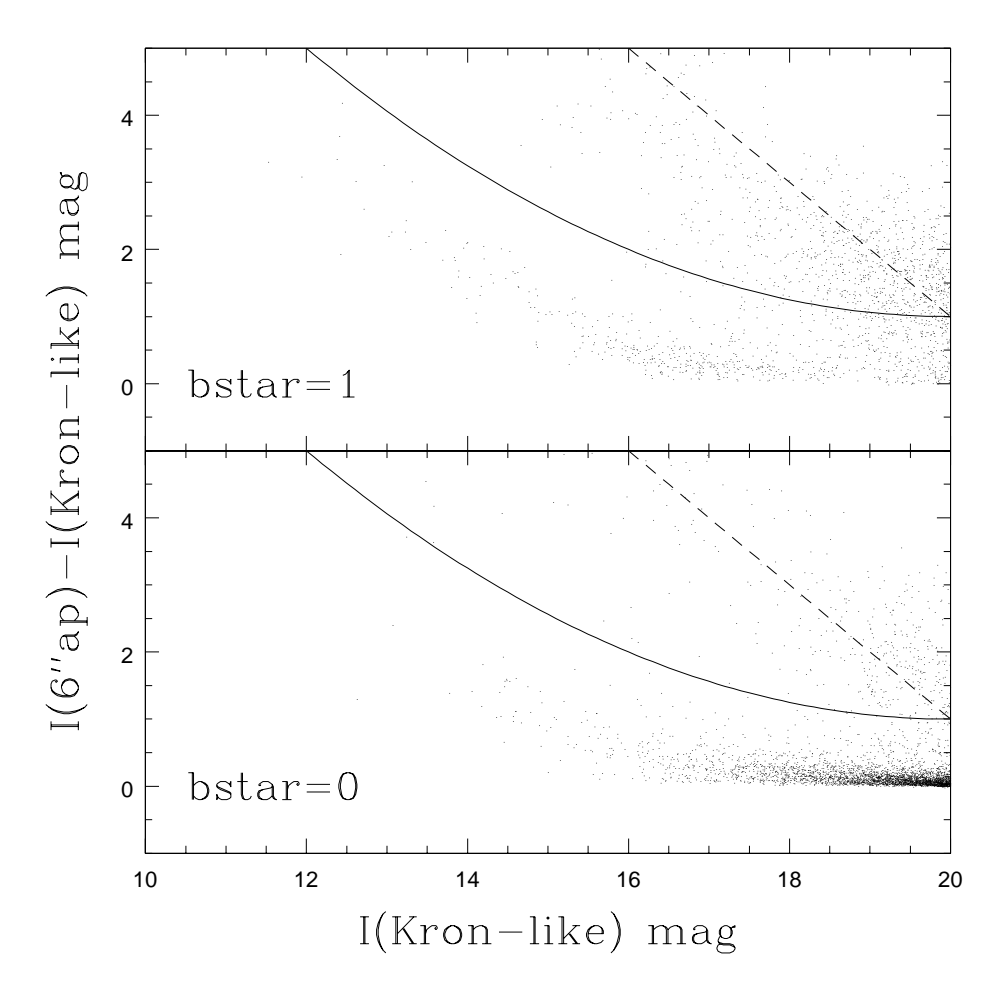


Fig. 3.— NDWFS bright star photometry problems. The top panel shows the difference between the I(6"0) aperture magnitude and the Kron-like (mag\_auto) I magnitudes for 5000 randomly selected galaxies near bright USNO stars (bstar = 1). The bottom panel shows the same quantities for 5000 galaxies which are not (bstar = 0). The Kron-like I band magnitudes tend to be overestimated when the source is close to a bright star. This is not true of the R band magnitudes used in the first season. All galaxies are required to have  $I_{ap6} < 21$  mag, which is indicated by the dashed line, while those close to bright stars are eliminated if  $r < R_{bstar}/2$  or if  $R_{bstar}/2 < r < R_{bstar}$  and they lie above the solid line,  $I_{ap6} > I + 1 + 4 \left[ (I - 20)/8 \right]^2$  mag.

(qcode05) samples where  $code05 = qcode05 + 128 \times gcode05$ .

- SDSS Calibration Stars: (code05 = 1): These are SDSS stars with the colors of F stars that are used to flux calibrate the spectra.
- Brown Dwarf Candidates: (code05 = 2, qcode05 = 1): These are the same brown dwarf candidates as in 2004, and we do not discuss them further.
- Optical Quasar Candidates: (code05 = 4, qcode05 = 2): These are  $B_W/R/I/K$ -band color-selected quasar candidates from an experiment by K. Brand and R. Green. The first class of targets consists of point sources with  $I K \ge 0.5 + (4.0/5.8)(B_W R)$  or I K > 3. The second class of objects consist of  $B_W$  non-detections which satisfy one of R I < 1.0, I K > 1.1 + (R I) or I K > 3.0. This was a small sample designed to test the color selection method and we do not discuss it further.
- WSRT Radio Sources: (code05 = 8, qcode05 = 4): All sources (qso = 1 or galaxy = 1) within 3".0 of a  $5\sigma$  detection in the WSRT 1.4 GHz survey of the field (de Vries et al. 2002). We made no attempt to deal with the problem of radio lobes other than to select unresolved sources in the de Vries et al. (2002) catalogs.
- X-ray Quasar Candidates: (code05 = 16, qcode05 = 8): All sources (qso = 1 or galaxy = 1) with 2 or more X-ray counts and a greater than 25% Bayesian probability of being identified with the optical source using the matching approach outlined in Brand et al. (2006). Remember that the optical flux limits are different for the extended and point-like targets.
- MIPS Quasar Candidates: (code05 = 32, qcode05 = 16): All point sources with  $F_{24} \ge 0.3$  mJy and I(3".0) >  $18 2.5 \log(F_{24}/\text{mJy})$ . We changed to using an I-band/24 $\mu$ m criterion to eliminate stars rather than a J-band/24 $\mu$ m criterion. Also note that the MIPS flux limit is below the 80% completeness limit of the 24 $\mu$ m catalogs. Fig. 4 illustrates this selection method.
- IRAC Quasar Candidates: (code05 = 64, qcode05 = 32): This sample includes both galaxies
  and point sources, with the standard optical flux limits of I ≤ 20 for the extended sources
  and I ≤ 21.5 for the point sources. The selection criteria are based on Stern et al. (2005),
  but have been modified to be more liberal for point sources and slightly more conservative
  for extended sources.
  - Point sources: Point sources brighter than  $[3.6]_{[3.6]} \le 18$  mag only needed to satisfy the criterion that  $[3.6]_{[3.6]}(3''.0) [4.5]_{[4.5]}(3''.0) \ge 0.4$  mag because we need only differentiate quasars from stars with (Vega) mid-IR colors of zero. For fainter point sources, where the color errors become significant, we added the requirement that the source had a measured  $[5.8]_{[5.8]}(3''.0)$  or  $[8.0]_{[8.0]}(3''.0)$  magnitude.

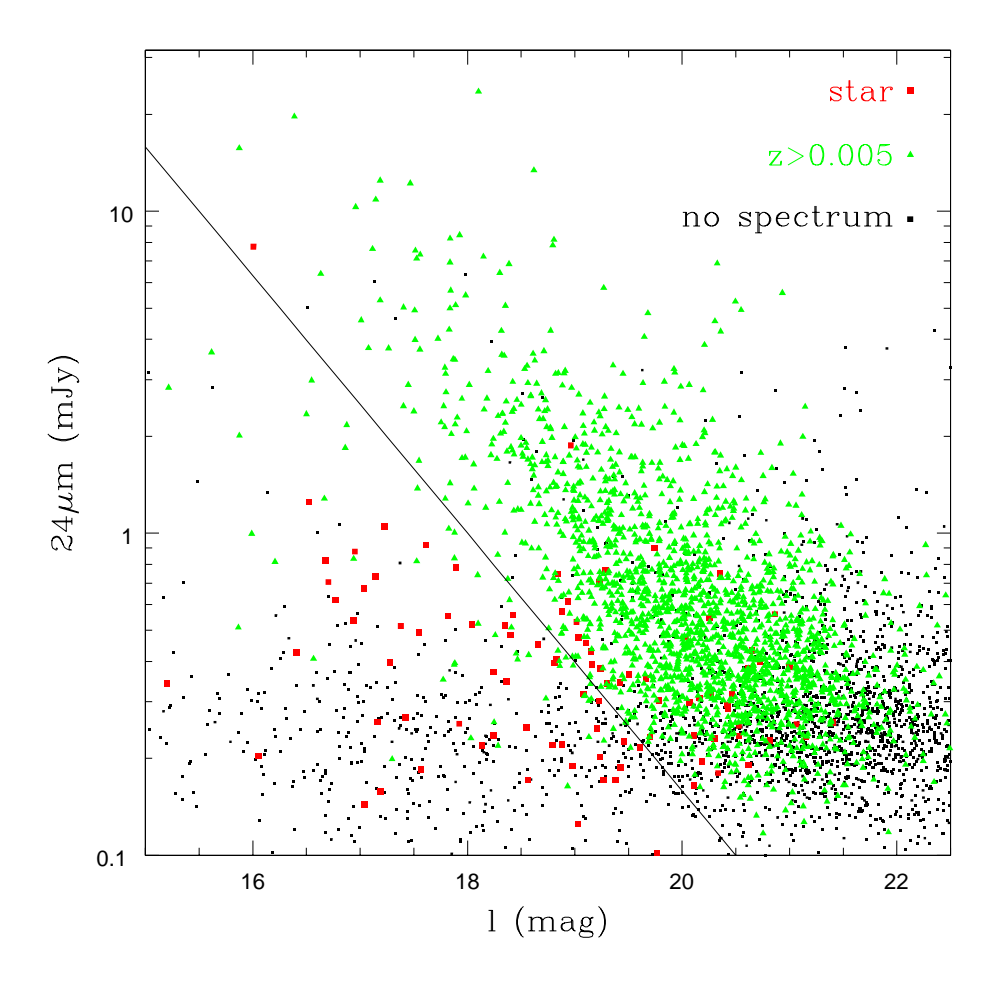


Fig. 4.— MIPS quasar selection. MIPS quasar targets are point sources with  $I(3''0) > 18 - 2.5 \log(F_{24}/mJy)$ . The green filled triangles show extragalactic sources, the filled red squares show stars, and the black squares are sources without spectroscopic confirmations. The black line indicates the color selection boundary. Targets appear below the line because of other targeting criteria.

- Extended Sources: Extended sources had to be detected in all four IRAC bands and satisfy the IRAC color cuts (these are all 3".0 aperture magnitudes)
  - \*  $[5.8]_{[5.8]} [8.0]_{[8.0]} > 0.6$ ,
  - \*  $[3.6]_{[3.6]} [4.5]_{[4.5]} > 0.2([5.8]_{[5.8]} [8.0]_{[8.0]}) + 0.4$  and
  - $* \ [3.6]_{[3.6]} [4.5]_{[4.5]} > 2.5 \left( [5.8]_{[5.8]} [8.0]_{[8.0]} \right) 3.5.$
- MIPS  $24\mu \text{m}$  Galaxy Sample: (code05 = 128, gcode05 = 1): This sample consists of galaxies (galaxy = 1) with  $F_{24} \ge 0.3$  mJy. We attempted to obtain redshifts of all galaxies with  $F_{24} \ge 0.5$  mJy and a randomly selected 30% (rcode  $\le 5$ ) of the galaxies with  $0.3 \le F_{24} < 0.5$  mJy. Note that these  $24\mu \text{m}$  flux limits are fainter than the 80% completeness limit of the  $24\mu \text{m}$  catalogs.
- IRAC Channel 4 (8.0 $\mu$ m) Galaxy Sample: (code05 = 256, gcode05 = 2): This sample consists of galaxies (galaxy = 1) with [8.0]<sub>[8.0]</sub>  $\leq$  13.8 mag. We attempted to obtain redshifts of all galaxies with [8.0]<sub>[8.0]</sub>  $\leq$  13.2 mag and a randomly selected 30% (rcode  $\leq$  5) of the galaxies with 13.2 < [8.0]<sub>[8.0]</sub>  $\leq$  13.8 mag.
- IRAC Channel 3 (5.8 $\mu$ m) Galaxy Sample: (code05 = 512, gcode05 = 4): This sample consists of galaxies (galaxy = 1) with [5.8]<sub>[5.8]</sub>  $\leq$  15.2 mag. We attempted to obtain redshifts of all galaxies with [5.8]<sub>[5.8]</sub>  $\leq$  14.7 mag and a randomly selected 30% (rcode  $\leq$  5) of the galaxies with 14.7 < [5.8]<sub>[5.8]</sub>  $\leq$  15.2 mag.
- IRAC Channel 2 (4.5 $\mu$ m) Galaxy Sample: (code05 = 1024, gcode05 = 8): This sample consists of galaxies (galaxy = 1) with [4.5]<sub>[4.5]</sub>  $\leq$  15.7 mag. We attempted to obtain redshifts of all galaxies with [4.5]<sub>[4.5]</sub>  $\leq$  15.2 mag and a randomly selected 30% (rcode  $\leq$  5) of the galaxies with 15.2 < [4.5]<sub>[4.5]</sub>  $\leq$  15.7 mag.
- IRAC Channel 1 (3.6 $\mu$ m) Galaxy Sample: (code05 = 2048, gcode05 = 16): This sample consists of galaxies (galaxy = 1) with [3.6]<sub>[3.6]</sub>  $\leq$  15.7 mag. We attempted to obtain redshifts of all galaxies with [3.6]<sub>[3.6]</sub>  $\leq$  15.2 mag and a randomly selected 30% (rcode  $\leq$  5) of the galaxies with 15.2 < [3.6]<sub>[3.6]</sub>  $\leq$  15.7 mag.
- GALEX FUV-band Galaxy Sample: (code05 = 4096, gcode05 = 32): This sample consists of galaxies (galaxy = 1) with FUV ≤ 22.5 mag. We attempted to obtain redshifts of all galaxies with FUV ≤ 22.0 mag and a randomly selected 30% (rcode ≤ 5) of the galaxies with 22.0 < FUV ≤ 22.5 mag. The GALEX data available at the time covered only a small fraction of the standard fields.
- GALEX NUV-band Galaxy Sample: (code05 = 8192, gcode05 = 64): This sample consists of galaxies (galaxy = 1) with NUV  $\leq$  22.0 mag. We attempted to obtain redshifts of all galaxies with NUV  $\leq$  21.0 mag and a randomly selected 30% (rcode  $\leq$  5) of the galaxies with 21.0 < NUV  $\leq$  22.0 mag.

- K-band Galaxy Sample: (code05 = 16384, gcode05 = 128): This sample consists of galaxies (galaxy = 1) with either NDWFS K/K<sub>s</sub> or FLAMEX K<sub>s</sub>  $\leq$  16.5 mag. We attempted to obtain redshifts of all galaxies with K  $\leq$  16.0 mag and a randomly selected 20% (rcode  $\leq$  3) of the galaxies with 16.0 < K  $\leq$  16.5 mag.
- J-band Galaxy Sample: (code05 = 32768, gcode05 = 256): This sample consists of galaxies (galaxy = 1) with FLAMEX J  $\leq$  18.5 mag. We attempted to obtain redshifts of all galaxies with J  $\leq$  17.5 mag and a randomly selected 20% (rcode  $\leq$  3) of the galaxies with 17.5 < B<sub>W</sub>  $\leq$  18.5 mag.
- $B_W$ -band Galaxy Sample: (code05 = 65536, gcode05 = 512): This sample consists of galaxies (galaxy = 1) with  $B_W \le 21.3$ . We attempted to obtain redshifts of all galaxies with  $B_W \le 20.5$  mag and a randomly selected 20% (rcode  $\le 3$ ) of the galaxies with 20.5  $< B_W \le 21.3$  mag. The bright ( $B_W < 20.5$ ) part of this sample should be very similar to the 2004  $B_W$ -band galaxy sample (code04 = 64).
- R-band Galaxy Sample: (code05 = 131072, gcode05 = 1024): This sample consists of galaxies (galaxy = 1) with R  $\leq$  20. We attempted to obtain redshifts of all galaxies with R  $\leq$  19.2 mag and a randomly selected 20% (rcode  $\leq$  3) of the galaxies with 19.2 < R  $\leq$  20 mag. This sample should be very similar to the 2004 R-band galaxy sample (code04 = 2048 plus code04 = 512).
- Other I-band Galaxies: (code05 = 262144, gcode05 = 2048): This sample consists of all galaxies (galaxy = 1) with I  $\leq$  20 mag that were not included in the Main I-band Galaxy sample. These sources were observed at lower priority than the main samples. Galaxies with lower rcode values are preferentially observed to make it easier for any later survey to produce larger randomly selected sub-samples.
- Main I-band Galaxy Sample: (code05 = 524288, gcode05 = 4096): This sample consists of galaxies (galaxy = 1) with I  $\leq$  20. We attempted to obtain redshifts of all galaxies with 15  $\leq$  I  $\leq$  18.5 mag and a randomly selected 20% (rcode  $\leq$  3) of the galaxies with 18.5 < I  $\leq$  20 mag.

### 2.6. 2006 and 2007 Sample Definitions

The 2006 sample definitions are very similar to those of 2005 except for changes in the AGN sample definitions to make use of the zBoötes data and to better characterize selection effects. The 2006 sample definitions were used again in 2007. The basic sample was selected from the I band catalog and then matched to all the other bands. The NDWFS optical photometry was flagged as good (bgood, rgood or igood = 1) if the Kron-like magnitude was defined (magnitude between 0 and 80), the SExtractor flags were FLAGS < 8 and the catalog duplication flag was FLAG\_DUPLICATE = 0. The criterion that photometric data was available (FLAG\_PHOT = 1) was dropped. For the z'-band, objects were flagged as good (zgood = 1) if the source was not split,

came from a region with more than 4 observations and was not flagged in the zBoötes catalog as being near a bright star. An object was defined as a point source, pntsrc = 1, if it had a SExtractor stellarity index  $\geq 0.8$  in any of the  $B_W$ , R, I or z'-bands with good data (bgood = 1 etc).

A galaxy target (galaxy = 1) was required to have pntsrc = 0, igood = 1 and one of rgood, bgood or zgood = 1. It then had to satisfy the (Kron-like) I-band magnitude criteria I  $\leq$  20 mag, 1".0 aperture magnitude  $I_{ap1} \leq 24.0$  and 6".0 aperture magnitude  $I_{ap6} \leq 21.0$ . A quasar target (qso = 1) had to have either igood = 1 or zgood = 1, which is more liberal than in 2005 because requirements on rgood or bgood could be problematic for very high redshift quasars. It then had to satisfy either that  $I \leq 22.5$  and a 1".0 aperture I-band magnitude  $I_{ap1} \leq 24$  mag or that  $z' \leq 22.5$  and a 1".0 z-band magnitude  $z'_{ap1} \leq 24.0$  mag. We also included a separate category AGN/galaxy (agngalaxy = 1) which was an extended source that did not have to meet the criterion on the 6".0 aperture magnitude and included sources down to the faint limit used for the point sources  $I \leq 22.5$  mag rather than the limit used for normal galaxies of  $I \leq 20$  mag. The limit on the aperture magnitude is designed to filter out problems created by bright stars.

- SDSS Calibration Stars: (code06 = 1): These are SDSS stars with the colors of F stars that are used to flux calibrate the spectra.
- Brown Dwarf Candidates: (code06 = 2, qcode06 = 1): These are brown dwarf candidates (M. Ashby, private communication). This sample is unchanged from 2005 other than through the modified definitions of galaxies and point sources.
- Optical Quasar Candidates: (code06 = 4, qcode06 = 2): These are  $B_W/R/I/K$ -band color-selected quasar candidates (Brand & Green, private communication). This sample is unchanged from 2005 other than through the modified definitions of galaxies and point sources.
- WSRT Radio Sources: (code06 = 8, qcode06 = 4): All sources (qso = 1, galaxy = 1, or agngalaxy = 1) within 3".0 of a  $5\sigma$  detection in the WSRT 1.4 GHz survey of the field (de Vries et al. 2002). This differs from 2005 by including the faint, extended sources with agngalaxy = 1.
- X-ray Quasar Candidates: (code06 = 16, qcode06 = 8): All sources (qso = 1, galaxy = 1, or agngalaxy = 1) with 2 or more X-ray counts and a greater than 25% Bayesian probability of being identified with the optical source using the matching approach outlined in Brand et al. (2006). This differs from 2005 by including the faint, extended sources with agngalaxy = 1.
- MIPS Quasar Candidates: (code06 = 32, qcode06 = 16): This sample is unchanged from 2005 other than through the modified definitions of galaxies and point sources.
- IRAC Quasar Candidates: (code06 = 64, qcode06 = 32): This sample is the most heavily modified from 2005. The changes were implemented to better understand selection effects due to color and morphology. For point sources, it was clear from detailed analyses that the old

color criterion led to reduced completeness whenever a bright emission line was in the  $3.6\mu m$  band, in particular at  $z \sim 4.5$  with the H $\alpha$  line (see Assef et al. 2010). It was also clear that the differing magnitude limits for point and extended sources were a significant problem at low redshifts. The new selection criterion were sufficiently complex that we introduced a separate code (iracq06) to label the various criteria. We also switched to using colors measured with positions set by the  $3.6\mu m$  band ([x]<sub>[3.6]</sub> magnitudes rather than [x] $_x$  magnitudes).

- iracq06 = 1: Point sources brighter than  $[3.6]_{[3.6]} \le 18$  mag with  $[3.6]_{[3.6]}(3''.0) [4.5]_{[3.6]}(3''.0) \ge 0.4$  mag. This differs from 2005 only in using the same band to set the position of the aperture by using  $[4.5]_{[3.6]}$  instead of  $[4.5]_{[4.5]}$ .
- iracq06 = 2: Point sources in the magnitude range  $18.0 < [3.6]_{[3.6]} ≤ 18.5$  mag with  $[3.6]_{[3.6]}(3''0) [4.5]_{[3.6]}(3''0) ≥ 0.4$  mag and either  $I(3''0) [3.6]_{[3.6]}(3''0) ≥ 3$  or  $z'(3''0) [3.6]_{[3.6]}(3''0) ≥ 3$ . The latter two criteria were included to minimize stellar contamination without requiring a detection in the less sensitive 5.8 or  $8.0\mu$ m IRAC bands.
- iracq06 = 3: The point source criteria for irac06 = 1 or 2 can lose objects when strong emission lines pass through the 3.6 $\mu$ m band, particularly at  $z \sim 4.5$  (H $\alpha$ ). To minimize stellar contamination, we added objects with  $[3.6]_{[3.6]} \leq 18.0$  and  $[3.6]_{[3.6]}(3''.0) [4.5]_{[3.6]}(3''.0) \geq 0.3$  mag subject to the added criterion on the optical to mid-IR color that either  $I(3''.0) [3.6]_{[3.6]}(3''.0) \geq 3$  or  $z'(3''.0) [3.6]_{[3.6]}(3''.0) \geq 3$ . We included 25% (rcode  $\leq 4$ ) of these sources at high priority, and the remainder at low priority.
- irac06 = 4: Extended sources flagged as standard galaxies (galaxy = 1, so I  $\leq$  20) had to be detected in all four IRAC bands and satisfy the IRAC color cuts

```
* [5.8]_{[3.6]}(3''.0) - [8.0]_{[3.6]}(3''.0) > 0.6,
```

\* 
$$[3.6]_{[3.6]}(3\rlap.{''}0) - [4.5]_{[3.6]}(3\rlap.{''}0) > 0.2([5.8]_{[3.6]}(3\rlap.{''}0) - [8.0]_{[8.0]}(1\rlap.{''}0)) + 0.4$$
 and

$$* \ [3.6]_{[3.6]}(3\rlap.{''}0) - [4.5]_{[3.6]}(3\rlap.{''}0) > 2.5 \left([5.8]_{[3.6]}(3\rlap.{''}0) - [8.0]_{[8.0]}(1\rlap.{''}0)\right) - 3.5.$$

This differs from 2005 only in using  $[x]_{[3.6]}$  rather than  $[x]_x$  to define the colors.

- irac06 = 5: Extended sources that were not flagged as standard galaxies (galaxy = 1 and thus extended sources with I  $\leq$  20), but were flagged as faint galaxies (agngalaxy = 1, so extended sources 20  $\leq$  I  $\leq$  22.5), were detected in all four IRAC bands and satisfied the IRAC color cuts
  - \*  $[5.8]_{[3.6]}(3''.0) [8.0]_{[3.6]}(3''.0) > 0.6,$
  - \*  $[3.6]_{[3.6]}(3\rlap.{''}0) [4.5]_{[3.6]}(3\rlap.{''}0) > 0.2([5.8]_{[3.6]}(3\rlap.{''}0) [8.0]_{[3.6]}(1\rlap.{''}0)) + 0.4$  and
  - $* \ [3.6]_{[3.6]}(3\rlap.{''}0) [4.5]_{[3.6]}(3\rlap.{''}0) > 2.5 \left([5.8]_{[3.6]}(3\rlap.{''}0) [8.0]_{[3.6]}(1\rlap.{''}0)\right) 3.5.$
- MIPS  $24\mu m$  Galaxy Sample: (code06 = 128, gcode06 = 1): This sample is unchanged from 2005 other than through the modified definitions of galaxies and point sources.
- IRAC Channel 4 (8.0 $\mu$ m) Galaxy Sample: (code06 = 256, gcode06 = 2): This sample is unchanged from 2005 other than through the modified definitions of galaxies and point sources.

- IRAC Channel 3 (5.8 $\mu$ m) Galaxy Sample: (code06 = 512, gcode06 = 4): This sample is unchanged from 2005 other than through the modified definitions of galaxies and point sources.
- IRAC Channel 2  $(4.5\mu\text{m})$  Galaxy Sample: (code06 = 1024, gcode06 = 8): This sample is unchanged from 2005 other than through the modified definitions of galaxies and point sources.
- IRAC Channel 1 (3.6 $\mu$ m) Galaxy Sample: (code06 = 2048, gcode06 = 16): This sample is unchanged from 2005 other than through the modified definitions of galaxies and point sources.
- GALEX FUV-band Galaxy Sample: (code06 = 4096, gcode06 = 32): This sample was rebuilt from the public GALEX catalogs available for the field in 2007, within 0.45 deg of the GALEX field center and with at least 2000 sec of NUV integration time. The GALEX data still covered only a modest fraction of the standard fields.
- GALEX NUV-band Galaxy Sample: (code06 = 8192, gcode06 = 64): This sample was rebuilt from the public GALEX catalogs available for the field in 2007, within 0.45 deg of the GALEX field center and with at least 2000 sec of NUV integration time.
- K-band Galaxy Sample: (code06 = 16384, gcode06 = 128): This sample is unchanged from 2005 other than through the modified definitions of galaxies and point sources.
- J-band Galaxy Sample: (code06 = 32768, gcode06 = 256): This sample is unchanged from 2005 other than through the modified definitions of galaxies and point sources.
- $B_W$ -band Galaxy Sample: (code06 = 65536, gcode06 = 512): This sample is unchanged from 2005 other than through the modified definitions of galaxies and point sources.
- R-band Galaxy Sample: (code06 = 131072, gcode06 = 1024): This sample is unchanged from 2005 other than through the modified definitions of galaxies and point sources.
- Other I-band Galaxies: (code06 = 262144, gcode06 = 2048): This sample is unchanged from 2005 other than through the modified definitions of galaxies and point sources.
- Main I-band Galaxy Sample: (code06 = 524288, gcode06 = 4096): This sample is unchanged from 2005 other than through the modified definitions of galaxies and point sources.

## 3. Observations

The observations were made with Hectospec (Fabricant et al. 1998, Roll et al. 1998, Fabricant et al. 2005), a 300 fiber, 1 degree field of view, robotic spectrograph for the 6.5m MMT telescope at Mt. Hopkins. The wavelength range is 3700Å to 9200Å with a pixel scale of 1.2Å and a spectral resolution of 6Å (i.e. roughly  $R \sim 1000$ ). The throughput at the wavelength extremes is low, and an

infrared LED in the fiber robots contaminates some spectra redward of 8500Å, with an amplitude that depends on the proximity of the fiber to the source. The fibers have a diameter of only 1".5. We generically aimed for 30 sky fibers, sometimes obtaining more if there was a shortage of targets, and 3–5 SDSS F-star candidates for flux calibration.

In 2004 we tried to put 20 of the sky fibers on blank sky positions selected from the SDSS imaging data for the field and the rest at random positions, but eventually switched to simply using random positions as it became clear that contamination of the sky fibers by sources was not a significant problem. In the first runs in 2004 the atmospheric dispersion corrector was not working properly (see Table 2), which means that some of the spectra could not be properly flux calibrated and there are significant spectral distortions unless the data was obtained very close to the zenith. The guide cameras are primarily red sensitive, so the fibers generally were properly positioned for the red light while the bluer wavelengths were systematically shifted, sometimes leading to quite dramatic losses for blue emission from point sources.

Observations are described by a three digit pass number ABB where, in general, A indicates the sequential pass over the fields and BB indicates the field. So pass 203 would be the second pointing at sub-field 3. The individual pointings were not exactly centered on the fields, but were shifted to help maximize the overall completeness. Weather problems, leading to repeated observations, the longevity of the project, and the introduction of coadded spectra from multiple observations eventually led to a partial break down in the naming scheme. Table 2 summarizes all the observations.

In 2004 we carried out three passes with integration times of 24, 45 and 75 minutes divided into 2, 3 and 4 exposures respectively. The targets were divided into surface brightness classes with the high, medium and low surface brightness targets assigned to the short, medium, and long integration times. Targets with failed redshifts in the first passes were recycled for observations in the later, deeper passes. The systematic recycling of failures during this and later seasons means that fiber collisions are largely irrelevant to the completeness of any of the AGES samples.

The 2005 observations used pass numbers of 4 through 7 indicating the month of the observation (March, April, May and June/July) and field numbers of  $1\cdots 26$  where  $1\cdots 15$  correspond to the standard sub-fields,  $16\cdots 21$  to observations in the boundary regions, and  $22\cdots 26$  to repeat observations in the 15 standard sub-fields. The exposure times were generally 90 minutes. Experiments using 54 minute exposure times had poor redshift yields. The observing conditions were not homogeneous, with significant variations in the signal-to-noise ratios beyond the effects of the changing exposure times.

In 2006 we had less time and terrible weather. All the observations were designated as pass 8, where in the first run we observed fields 1–5 (801, 802, 803, 804, 805). The poor yields led us to repeat these observations in the second run (these we labeled by the field number plus twenty, so 821, 822, 823, 824, 825, and 834 for observations of fields 1, 2, 3, 4, 5 and 14, and there was one additional observation of field 1 labeled 841). We also produced co-added spectra of all multiply

observed targets that were assigned codes of 861, 862, and 863. In 2007 we tried to focus on fields with lower completeness levels. These were numbered in the 900's, again adding 20 to the pass number when a field was re-observed.

Quasars with redshift z > 2.4 were repeatedly reobserved until the co-added spectrum yielded a signal-to-noise ratio above 10/pixel. The objective was to build a clean sample for potentially studying correlations in Ly $\alpha$  forest absorption. SDSS redshifts are marked as pass/aperture 0/0 entries.

#### 4. Data Reduction

The data were reduced by two separate pipelines, the standard Hectospec pipeline at the Center for Astrophysics (CfA) and a modified SDSS pipeline, HSRED.

In the CfA pipeline the separate exposures were de-biased and flat fielded using exposures of the MMT ceiling illuminated by a continuum lamp (the latter exposures had the lamp spectral shape removed by the IRAF program "apflatten"). The object exposures were then compared before extraction to allow identification and elimination of cosmic rays through interpolation. Spectra were then extracted from individual exposures using the variance weighting method, wavelength calibrated and combined. Each fiber has a distinct wavelength dependence in throughput, which can be estimated using flat field exposures or the twilight sky. The object spectra were next corrected for this dependence, followed by a correction to put all the spectra on the same exposure level. The latter correction was estimated by the strength of several night sky emission lines. Sky subtraction was performed, using object-free spectra as near as possible to each target. Small corrections to the wavelength zero point based on the wavelengths of night sky emission lines were then applied. Finally, redshifts were estimated by cross correlation with emission/absorption line galaxy and AGN template spectra. The CfA pipeline spectra are then the average of the extracted spectra in counts.

For HSRED, the observations of the flat-field screen taken in the afternoon were again used to correct for the high-frequency flat-field variations and fringing in the CCD. We removed low-frequency fiber-to-fiber transmission differences using observations of the twilight sky. Wavelength solutions were obtained each night using observations of HeNeAr calibration lamps, and the locations of strong emission lines in the spectrum of the night sky were used to correct for any drift in the wavelength solution between observations of the calibration frames and the data frames. Each Hectospec configuration has approximately 30 fibers dedicated to measuring the sky spectrum. These sky observations were used to create a median sky spectrum for each exposure which was interpolated and subtracted from each object spectrum. Simultaneous observations of F-type stars in each configuration were cross-correlated against a grid of Kurucz models (Kurucz 1993) to derive a sensitivity function for each observation, thus linking the observed counts to absolute flux units. Where flux calibration is successful, the HSRED spectra are  $F_{\lambda}$  in units of  $10^{-17}$  ergs cm<sup>-2</sup> s<sup>-1</sup> Å<sup>-1</sup>.

Redshifts were determined using programs available in the IDLSPEC2D package of IDL routines developed for the SDSS. To determine the redshift of each object in the survey, we compared the observed spectra with empirical stellar, galaxy, and quasar template models included in the IDLSPEC2D package and allowed the strength of the emission lines present in the object to be fit simultaneously with the redshift of the galaxy. The final redshift and object classification were determined by selecting the template and redshift combination that minimized the  $\chi^2$  between model and data.

All spectra were visually inspected, usually by two individuals (CSK and DJE), with a particular focus on low S/N spectra and spectra where the two pipelines produced discrepant redshifts. These were then either flagged as wrong, adjusted to the correct value or analyzed manually.

## 5. A Summary of the Survey

The general properties of the survey are summarized in Tables 1, 3 and 4 and illustrated in Figures 2, 5 and 6. Table 1 and Figure 2 illustrate the spatial completeness of the survey using the main I-band galaxy sample. In the standard sub-fields, spectra were attempted for 96.6% of this sample, and redshifts were measured for 93.6%. The completeness is worst for fields 13, 14 and 15, both in terms of the fraction of attempts (86% to 91%) and the overall completeness (83% to 89%). Two factors led to the lower completeness. First, all three of the fields have more targets (786, 748 and 855 respectively) than the mean (734 per field), although we achieved much higher completenesses for other dense fields such as field 4. Second, we emphasized completing the lower field numbers in the face of poor weather and limited time to finish our observations. Every field was observed many times (see Table 2), so fiber collisions play a very small role in the incompleteness.

Table 3 summarizes the 2006/2007 samples, excluding the flux calibration stars, brown dwarf and optical quasar test samples. The well-defined galaxy samples are very complete, with the main I-band sample having the lowest completeness (94%), followed by the MIPS sample (95%). The remainder have completenesses above 98%. The GALEX samples are spatially inhomogeneous and of limited use. In total, we obtained redshifts for roughly 61% of the galaxies with I < 20 mag.

Fig. 5 shows the completeness as a function of the random sample code. Because we emphasized observing lower rcodes, it is relatively easy to rapidly increase the size of the sample with high completeness. The main I-band galaxy sample used 20% sparse sampling (rcode  $\leq$  3) for its fainter magnitudes,  $18.5 \leq I \leq 20$ , while the IR samples used 30% sparse sampling (rcode  $\leq$  5). The higher rcodes were assigned priorities that dropped with every increase in the rcode by two, leading to the steady drop in the completeness. With this design, little effort is needed to produce significantly larger complete samples. About 500 redshifts are needed to complete the main galaxy sample. Another 1600 would complete the sample to a sparse sampling fraction between 18.5 < I < 20 of 40%.

In total we selected almost 8977 objects as AGN candidates, took spectra of 7102, and obtained

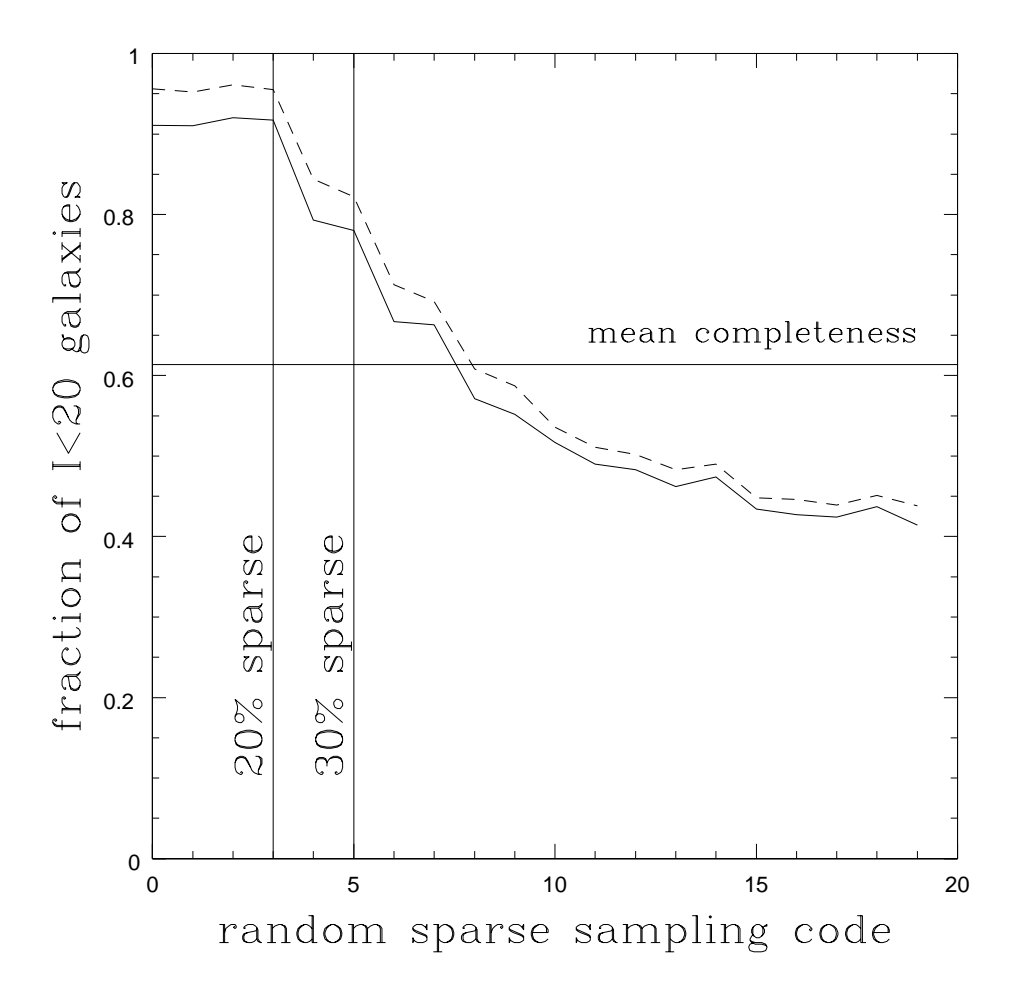


Fig. 5.— Completeness as a function of the random sparse sampling **rcode** (see  $\S 2.2$ ) for all I < 20 mag galaxies, where each rcode bin contains an average of 5% of the targets (1959 for the I < 20 mag galaxies). The dashed line indicates the fraction with spectra and the solid line the fraction with measured redshifts. The horizontal line shows the mean completeness and the vertical lines mark the 20% and 30% sparse sampling goals for the main I band sample and the other galaxy samples, respectively.

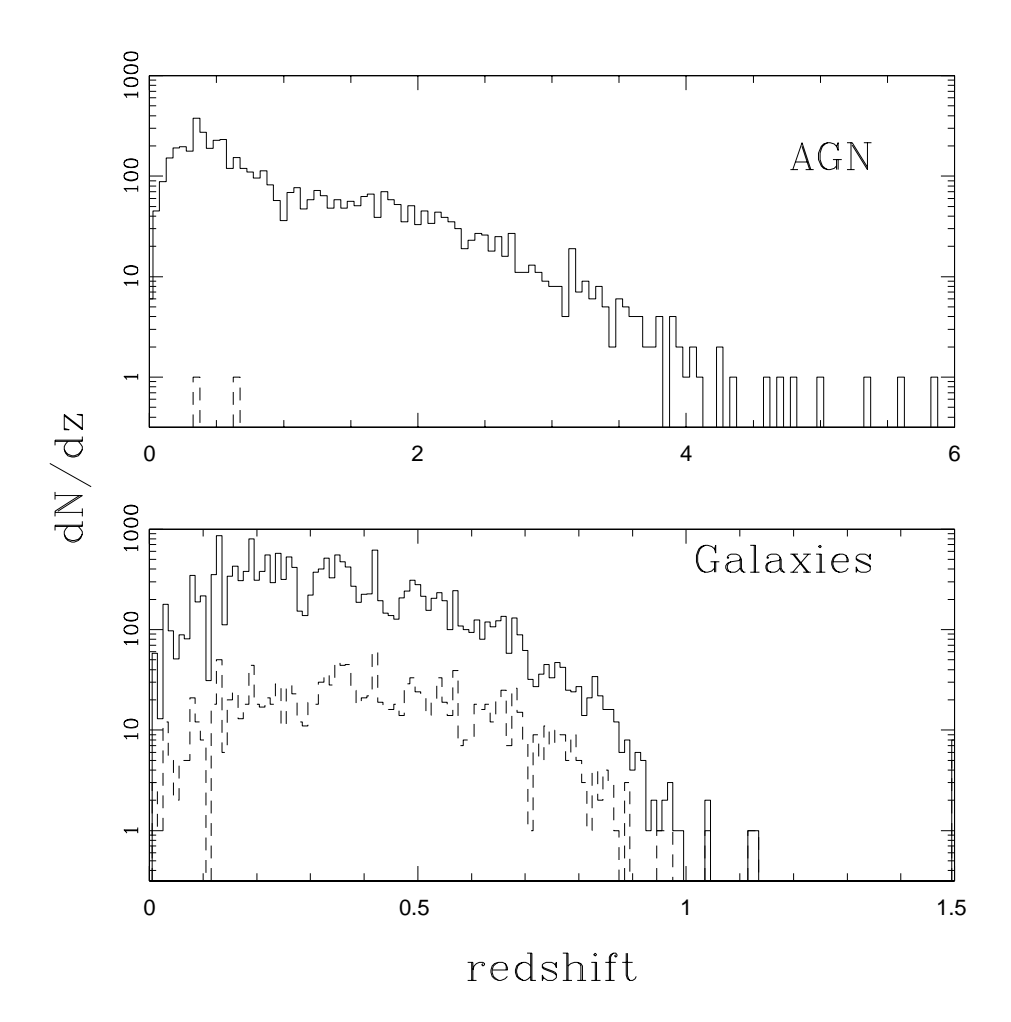


Fig. 6.— The redshift distributions of AGN (top) and galaxies (bottom). In the top panel the solid (dashed) histograms are for point (extended) sources with an AGN targeting code (qcode06 > 3). In the lower panel, the solid histograms shows all objects targeted as galaxies (gcode06 > 0), and the dashed histograms show the objects targeted as galaxies that also had an AGN targeting code (qcode06 > 3).

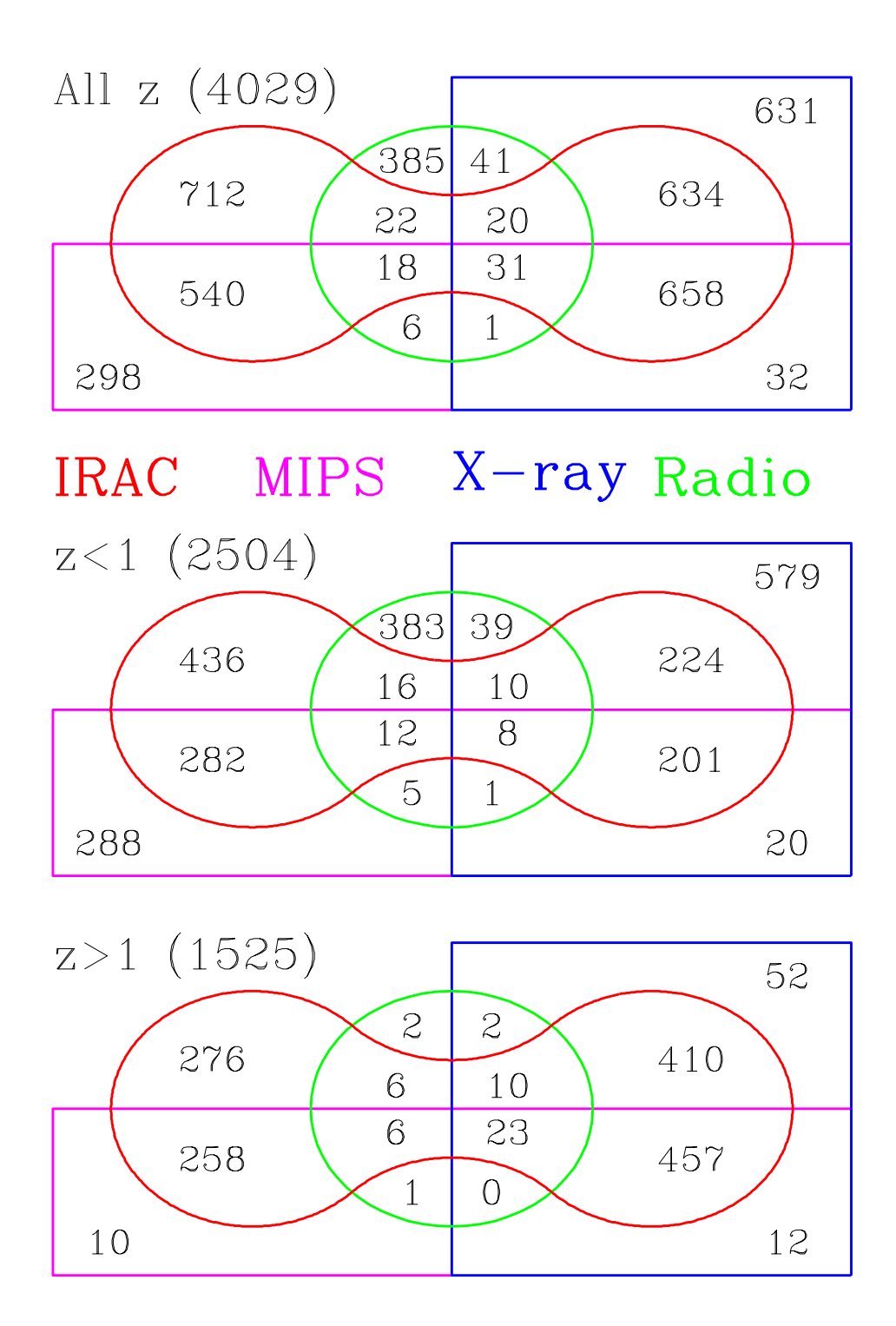


Fig. 7.— Venn diagrams illustrating the degree of overlap between the primary AGN selection methods (IRAC mid-IR, MIPS  $24\mu m$ , X-ray and radio). The panels show the divisions for all (top panel), lower redshift (z < 1, middle panel) and higher redshift (z > 1, lower panel) AGN. For any one of the selection methods, there are 8 possible overlaps ranging from no other method to all three other methods.

redshifts for 5217 of which 4764 were not Galactic stars. Table 4 summarizes the completeness of the various categories of AGN, breaking the statistics into the various sub-samples (point source, bright extended sources, faint extended sources) and giving statistics for all the AGN selection methods (all objects with an AGN selection code) as compared to the total galaxy sample (all objects with code06  $\geq$  128). In total, we identified 1718 AGN with z > 1 in the field, a surface density of more than 200/deg<sup>2</sup>. Three quasars with redshifts above 5 were identified (Cool et al. 2006). A redshift 6.12 quasar was targeted as an IRAC AGN but not observed before it was discovered by McGreer et al. (2006) and Stern et al. (2007). The completenesses for the point source and bright extended AGN are generally good, while that for the fainter extended AGN candidates is very poor. Fig. 6 shows the redshift distributions of the galaxy and AGN populations.

The different AGN selection methods emphasize different galaxy types and redshift ranges, as discussed in more detail by Hickox et al. (2007), Gorjian et al. (2008), Assef et al. (2010) and Assef et al. (2011). Fig. 7 illustrates some of these issues using a Venn diagram adapted from Assef et al. (2010) showing the overlap between the WSRT, X-ray, IRAC and MIPS quasar selection methods for several different redshift ranges. The primary difference between the X-ray (and radio) sample versus the IRAC and MIPS samples is that X-ray selection is essentially independent of host properties while the IRAC and MIPS samples are not. Thus, lower redshift AGN are more likely to be X-ray selected because the generally larger contribution of the host galaxy at lower redshifts changes the mid-IR colors or makes the optical counterpart to the MIPS source non-point-like. On the other hand, the mid-IR selection methods may well be better for finding moderately obscured quasars where the soft X-ray photons to which Chandra is most sensitive are absorbed. Many of these problems could be solved using the Assef et al. (2010) template models to fit the complete photometry for each source and target those with any evidence of an AGN contribution.

### 6. Data Release

The AGES data release consists of a series of row-matched tables. They do not contain all entries from the matched photometric catalogs, as these contain far more information than is needed to interpret the AGES data. We have also included only the final photometry used in later observing seasons. We do not report the photometry associated with the intermediate states because the completeness of the final samples is so high. We do report the selection codes used in the earlier observing seasons so that the history of the targeting can be traced if necessary and to explain the origin of the small numbers sources with redshifts that were not explicitly targeted in the final seasons.

Table 5 summarizes the selection codes for each source. This includes the 2004, 2005 and 2006/2007 targeting codes, the field IDs, the random sparse sampling code, the bright star flag, the IRAC AGN sub-sample code, and the flags for whether the source was considered a standard galaxy, a quasar, a point source, or a fainter galaxy that was an AGN candidate.

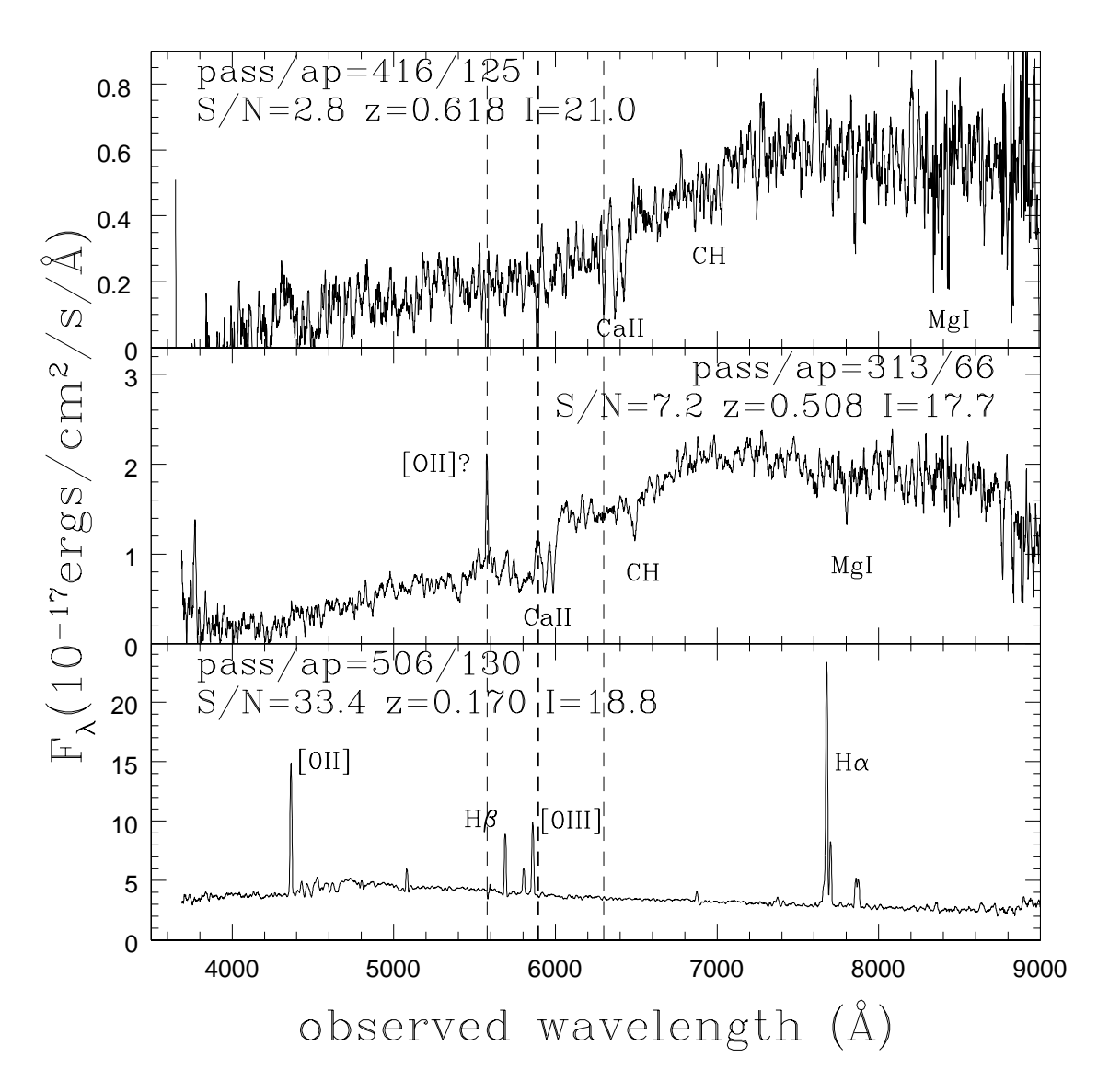


Fig. 8.— Three examples of the spectra of galaxies. The top, middle and lower panels show spectra with continuum signal-to-noise ratios typical of the worst 5%, median and best 5% of the spectra yielding redshifts. Several features are labeled, and the vertical lines mark the strong sky lines. The spectra are smoothed by an 11 pixel box car, which roughly halves the intrinsic spectral resolution.

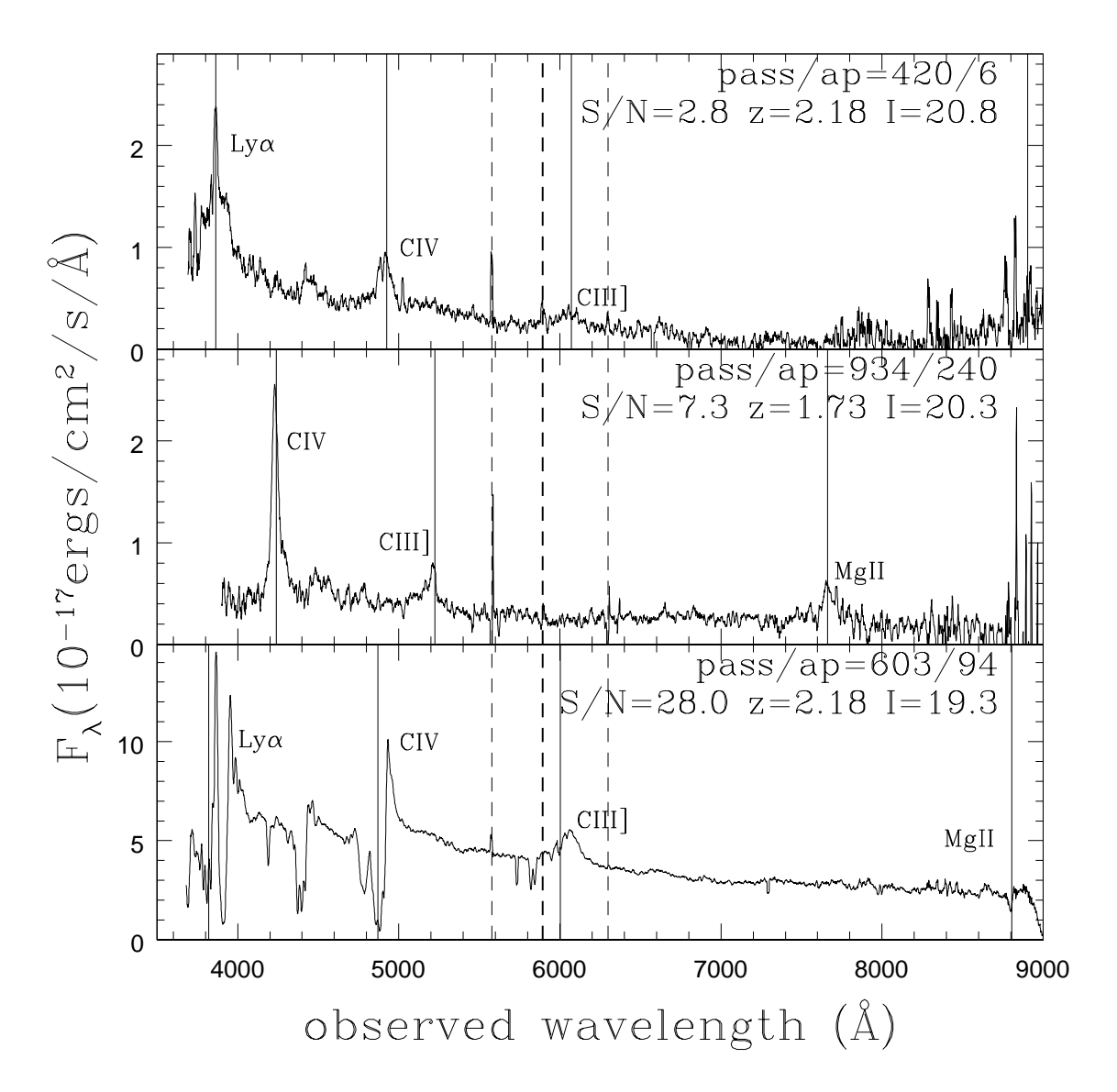


Fig. 9.— Three examples of the spectra of quasars. The top, middle and lower panels show spectra with continuum signal-to-noise ratios typical of the worst 5%, median and best 5% of the spectra yielding redshifts. Several features are labeled and marked by the solid vertical lines while the dashed lines mark the strongest sky lines. The spectra are smoothed by an 11 pixel box car. The strong (BAL) absorption features in the bottom spectrum have biased the pipeline redshift estimate.

Table 6 presents the photometry for the sources from XBoötes (Murray et al. 2005, Kenter et al. 2005, Brand et al. 2006), GALEX (Martin et al. 2005), NDWFS DR3 (Jannuzi & Dey 1999), zBoötes (Cool 2007), FLAMEX (Elston et al. 2006), the IRAC Shallow Survey (Eisenhardt et al. 2004) and Soifer & Spitzer/NOAO Team (2004). The X-ray photometry is in counts for sources with a 25% or greater Bayesian match probability in Brand et al. (2006). The NDWFS, FLAMEX and IRAC Shallow Survey are the (Kron-like/mag\_auto) Vega magnitudes, GALEX and zBoötes are in AB magnitudes, and the  $24\mu$ m flux is in mJy. Objects with unusual photometric properties should be inspected closely before use. Table 7 summarizes the spectroscopy, listing the number of spectra taken, the estimated redshifts, the (continuum) signal-to-noise ratio of the spectra, and the pass/aperture identification code for each spectrum. Figure 8 shows three examples of spectra of galaxies illustrating the quality for (continuum) signal-noise-ratios representative of the worst 5%, median and best 5% of the sample. Figure 9 does the same for three examples of quasar spectra. The signal-to-noise estimate in Table 7 is an indicator of redshift reliability, as well as any agreements/disagreements between repeated low signal-to-noise spectra.

Table 8 provides photometric redshift estimates and template decompositions for each object's photometry following Assef et al. (2010). The SED is fit as a combination of an early-type, late-type, star forming and (obscured) AGN for the full range of available UV/optical/near-IR/far-IR photometry, and we report the luminosities associated with each component and the extinction applied to the AGN template. Where a spectroscopic redshift is available, the template decomposition is carried out at the spectroscopic redshift. The accuracy of the photometric redshifts is  $\sigma_z = 0.04/(1+z)$  for galaxies, and Assef et al. (2010) should be consulted for a detailed discussion of the results for strong AGN. Finally, Table 9 presents the complete set of spectra in whatever form was available. This is somewhat heterogeneous in terms of pipeline and flux calibration, but a complete, homogeneous re-reduction of the data is beyond the scope of this paper.

As discussed in §4, the NDWFS Sextractor Kron-like magnitudes  $I_{AUTO}$  tend to overestimate source fluxes near bright stars. In Cool et al. (2011), we developed a method to produce a corrected estimate, which we summarize here. Let  $I_R = R_{AUTO} + (I(6\rlap.{''}0) - R(6\rlap.{''}0)))$  be the I-band magnitude predicted from the R-band Kron-like magnitude  $R_{AUTO}$  and the  $6\rlap.{''}0$  aperture color. The surrogate I-band total magnitude

$$I_{tot} = \frac{I_{AUTO} + I_R}{2} f + (1 - f) \max(I_{AUTO}, I_R)$$
 (1)

where  $f = \exp(-(I_{AUTO} - I_R)^2/0.2^2)$  is a weight factor. On average  $\langle I_{tot} - I_{AUTO} \rangle = 0.005$  mag with an rms scatter of 0.02 mag, but 10% (5%) of galaxies have shifts of 0.1 (0.5) mag.

Completeness corrections for the galaxy samples are relatively straightforward. Cool et al. (2011) discusses several tests of the completeness of the input catalogs, coming to the conclusion that the catalog completeness is of order 96-97%, largely due to the loss of faint objects superposed on brighter galaxies or stars. There are very few spurious objects. Only 1% of the main-sample galaxies lack counterparts in SDSS imaging, although some saturated stars were mis-identified as galaxy targets. These are easily identified because the resulting spectra and redshifts are stellar.

The remaining issues are the sparse sampling fractions, fiber allocation completeness and redshift failure rates. Following Cool et al. (2011), Table 10 provides the completeness corrections for the galaxy samples as well as the maximum redshift at which the galaxy would have entered the AGES sample and the corresponding volume  $V_{max}$  in the survey.

# 7. Discussion

In summary, the AGN and Galaxy Evolution Survey has measured approximately 23745 redshifts in the Boötes field of the NDWFS using a layered approach to target selection that produced well-defined samples of galaxies and AGN over a broad wavelength range. Here we have outlined the selection functions used during the survey, summarized the general properties of the resulting samples, and released the redshift data with a sketch of the underlying photometry. For the full set of photometric data, users must consult the original surveys.

AGES contains well-defined, highly complete galaxy samples in the optical  $B_W$ , R and I bands, the near-IR J and K/K<sub>s</sub> bands, and the mid-IR IRAC and MIPS 24 $\mu$ m bands. These have been used to derive luminosity functions and their evolution in the optical (Cool et al. 2011), all four IRAC bands (Dai et al. 2009) and at 24 $\mu$ m (Huang et al. 2007, Rujopakarn et al. 2010). The extensive redshift information can then be used to calibrate and test photometric redshifts (Brodwin et al. 2006, Brown et al. 2007, Assef et al. 2008, Assef et al. 2010, Hildebrandt et al. 2010) that can then be used to search for high redshift clusters in the field (Eisenhardt et al. 2008). Combining the broad range of source types, extensive photometry and large number of redshifts Assef et al. (2008) and Assef et al. (2010) built SED template models covering the range  $0.1\mu$ m to  $24\mu$ m for both galaxies and quasars. The set of four templates can describe almost all the sources in the sample well, and can be easily adapted to other filter systems.

The AGES redshift data has also been used to help estimate bolometric corrections from the mid to far-IR (Bavouzet et al. 2008), where there have been significant questions about how to correct from  $24\mu m$  fluxes to total far-IR fluxes. Watson et al. (2009) used it to estimate the X-ray properties of otherwise undetected galaxies and AGN, using "stacking" to estimate the contribution of AGN and star formation to X-ray emission as a function of cosmic epoch. Brand et al. (2009) used it to explore the origin of  $24\mu m$  emission in otherwise early-type galaxies, and Atlee et al. (2009) used it to study the evolution of the UV upturn in early-type galaxies.

The initial AGES data were used to develop a remarkably successful mid-IR approach to quasar selection by Stern et al. (2005). This approach was then used in the later years not only to build the largest existing sample of mid-IR-selected AGN, but also to explore its properties and limitations in detail both through other AGES mid-IR target samples (Assef et al. 2010, Assef et al. 2011) and comparisons with X-ray sources (Gorjian et al. 2008, Hickox et al. 2007, Assef et al. 2011). Hickox et al. (2007), Hickox et al. (2009) and Starikova et al. (2011) use the AGES data to explore the relationships between AGN accretion and galaxy properties and clustering, while

Kollmeier et al. (2006) examined the Eddington ratio distribution of quasars to find that the distributions were surprisingly narrow. Brown et al. (2006) and Assef et al. (2011) examine quasar luminosity functions using mid-IR and X-ray selected samples.

AGES was also used to help design aspects of SDSS-III (Eisenstein et al. 2011). Finally, the existence of the extensive AGES data has also helped motivate further studies of the Boötes field. The Spitzer Deep, Wide-Field Survey (SDWFS, Ashby et al. 2009) doubled the depth of the original IRAC Shallow Survey (Eisenhardt et al. 2004), while simultaneously enabling the first large scale extragalactic study of the mid-IR variability of AGN (Kozłowski et al. 2010a) and the serendipitous discovery of a highly luminous but obscured supernova (Kozłowski et al. 2010b). In the MIPS AGN and Galaxy Evolution Survey (MAGES, Jannuzi et al. 2011, in prep), the MIPS 24, 70 and  $160\mu m$  data for the field were similarly improved. The field has also been imaged by Herschel as a GTO program.

We thank the Hectospec instrument team and all the MMT Hectospec queue observers for making this project possible. We also thank T. Soifer, D. Weedman, J. Houck, M. Rieke and collaborators for permission to use the results of their GTO Spitzer/MIPS survey of the Boötes field. RJA is supported by an appointment to the NASA Postdoctoral Program a the Jet Propulsion Laboratory, administered by Oak Ridge Associated Universities through a contract with NASA. BTJ and AD are supported by the NSF through its funding of NOAO, which is operated for the NSF by AURA under a cooperative agreement. CJ, SSM and WRF acknowledge support from the Smithsonian Institution and by NASA contracts NAS8-38248, NAS8-01130, NAS8-39073, and NAS8-03060, and NASA grant GO3-4176A. Observations reported here were obtained at the MMT Observatory, a joint facility of the Smithsonian Institution and the University of Arizona. This work made use of images and/or data products provided by the NOAO Deep Wide-Field Survey, which is supported by the National Optical Astronomy Observatory (NOAO). NOAO is operated by AURA, Inc., under a a cooperative agreement with the National Science Foundation. This work is based in part on observations made with the Spitzer Space Telescope, which is operated by the Jet Propulsion Laboratory, California Institute of Technology under a contract with NASA. Support for this work was provided by NASA through an award issued by JPL/Caltech.

MMT, Spitzer, Chandra, GALEX, VLA, Mayall

#### REFERENCES

Abazajian, K. N., Adelman-McCarthy, J. K., Agüeros, M. A., et al. 2009, ApJS, 182, 543

Ashby, M. L. N., et al. 2009, ApJ, 701, 428

Assef, R. J., et al. 2008, ApJ, 676, 286

Assef, R. J., et al. 2010, ApJ, 713, 970

Assef, R. J., et al. 2011, ApJ, 728, 56

Atlee, D. W., Assef, R. J., & Kochanek, C. S. 2009, ApJ, 694, 1539

Bavouzet, N., Dole, H., Le Floc'h, E., Caputi, K. I., Lagache, G., & Kochanek, C. S. 2008, A&A, 479, 83

Becker, R. H., White, R. L., & Helfand, D. J. 1995, ApJ, 450, 559

Bell, E. F., McIntosh, D. H., Katz, N., & Weinberg, M. D. 2003, ApJS, 149, 289

Bertin, E., & Arnouts, S., 1996, A&AS, 117, 393

Blanton, M. R., & Roweis, S. 2007, AJ, 133, 734

Brand, K., et al. 2006, ApJ, 641, 140

Brand, K., et al. 2009, ApJ, 693, 340

Brodwin, M., et al. 2006, ApJ, 651, 791

Brown, M. J. I., Dey, A., Jannuzi, B. T., Brand, K., Benson, A. J., Brodwin, M., Croton, D. J., & Eisenhardt, P. R., 2007, ApJ, 654, 858

Brown, M. J. I., et al. 2006, ApJ, 638, 88

Colless, M., Dalton, G., Maddox, S., et al. 2001, MNRAS, 328, 1039

Cool, R. J., et al. 2006, AJ, 132, 823

Cool, R. J., et al. 2011, ApJ, submitted

Cool, R. J. 2007, ApJS, 169, 21

Cooper, M. C., Coil, A. L., Gerke, B. F., et al. 2010, MNRAS, 409, 337

Cowie, L. L., Songaila, A., Hu, E. M., & Cohen, J. G. 1996, AJ, 112, 839

Cowie, L. L., Barger, A. J., Fomalont, E. B., & Capak, P. 2004, ApJ, 603, L69

Croom, S. M., Smith, R. J., Boyle, B. J., et al. 2004, MNRAS, 349, 1397

Daddi, E., Renzini, A., Pirzkal, N., et al. 2005, ApJ, 626, 680

Dai, X., et al. 2009, ApJ, 697, 506

de Lapparent, V., Geller, M. J., & Huchra, J. P. 1986, ApJ, 302, L1

de Vries, W. H., Morganti, R., Röttgering, H. J. A., Vermeulen, R., van Breugel, W., Rengelink, R., & Jarvis, M. J. 2002, AJ, 123, 1784

Eisenhardt, P. R., et al. 2004, ApJS, 154, 48

Eisenhardt, P. R. M., et al. 2008, ApJ, 684, 905

Eisenstein, D. J., Weinberg, D. H., Agol, E., et al. 2011, AJ, 142, 72

Elston, R. J., et al. 2006, ApJ, 639, 816

Faber, S. M., Willmer, C. N. A., Wolf, C., et al. 2007, ApJ, 665, 265

Fabricant, D. G., Hertz, E. N., Szentgyorgyi, A. H., Fata, R. G., Roll, J. B., & Zajac, J. M. 1998, Proc. SPIE, 3355, 285

Fabricant, D., et al. 2005, PASP, 117, 1411

Giavalisco, M., Ferguson, H. C., Koekemoer, A. M., et al. 2004, ApJ, 600, L93

Gorjian, V., et al. 2008, ApJ, 679, 1040

Hickox, R. C., et al. 2007, ApJ, 671, 1365

Hickox, R. C., et al. 2009, ApJ, 696, 891

Hildebrandt, H., Arnouts, S., Capak, P., et al. 2010, A&A, 523, A31

Hopkins, A. M., & Beacom, J. F. 2006, ApJ, 651, 142

Huang, J.-S., et al. 2007, ApJ, 664, 840

Jannuzi, B. T., & Dey, A. 1999, The Hy-Redshift Universe: Galaxy Formation and Evolution at High Redshift, 193, 258

Kenter, A., et al. 2005, ApJS, 161, 9

Kollmeier, J. A., et al. 2006, ApJ, 648, 128

Kozłowski, S., et al. 2010, ApJ, 716, 530

Kozłowski, S., et al. 2010, ApJ, 722, 1624

Le Fèvre, O., Vettolani, G., Garilli, B., et al. 2005, A&A, 439, 845

Le Floc'h, E., Papovich, C., Dole, H., et al. 2005, ApJ, 632, 169

Martin, D. C., Fanson, J., Schiminovich, D., et al. 2005, ApJ, 619, L1

McGreer, I. D., Becker, R. H., Helfand, D. J., & White, R. L. 2006, ApJ, 652, 157

Murray, S. S., et al. 2005, ApJS, 161, 1

Reid, I. N., Brewer, C., Brucato, R. J., et al. 1991, PASP, 103, 661

Richards, G. T., Croom, S. M., Anderson, S. F., et al. 2005, MNRAS, 360, 839

Richards, G. T., Strauss, M. A., Fan, X., et al. 2006, AJ, 131, 2766

Roll, J. B., Fabricant, D. G., & McLeod, B. A. 1998, Proc. SPIE, 3355, 324

Rowan-Robinson, M., Babbedge, T., Oliver, S., et al. 2008, MNRAS, 386, 697

Rujopakarn, W., et al. 2010, ApJ, 718, 1171

Scodeggio, M., Vergani, D., Cucciati, O., et al. 2009, A&A, 501, 21

Scoville, N., Aussel, H., Brusa, M., et al. 2007, ApJS, 172, 1

Shectman, S. A., Landy, S. D., Oemler, A., et al. 1996, ApJ, 470, 172

Skrutskie, M. F., Cutri, R. M., Stiening, R., et al. 2006, AJ, 131, 1163

Soifer, B. T., & Spitzer/NOAO Team 2004, Bulletin of the American Astronomical Society, 36, 746

Starikova, S., Cool, R., Eisenstein, D., et al. 2011, ApJ, 741, 15

Stern, D., et al. 2005, ApJ, 631, 163

Stern, D., et al. 2007, ApJ, 663, 677

Voges, W., Aschenbach, B., Boller, T., et al. 1999, A&A, 349, 389

van Dokkum, P. G., Whitaker, K. E., Brammer, G., et al. 2010, ApJ, 709, 1018

Watson, C. R., et al. 2009, ApJ, 696, 2206

Werner, M. W., Roellig, T. L., Low, F. J., et al. 2004, ApJS, 154, 1

York, D. G., Adelman, J., Anderson, J. E., Jr., et al. 2000, AJ, 120, 1579

This preprint was prepared with the AAS IATEX macros v5.2.

Table 1. The Standard Fields

Field	RA	Dec	Main Galaxy Sample						
			Sample	Spectra Redshifts		Completeness			
1	216.750000	35.365000	774	772	753	97.3%			
2	216.666667	34.578889	751	750	731	97.3%			
3	216.766667	33.838333	729	723	710	97.4%			
4	216.629167	33.121389	911	902	861	94.5%			
5	217.404167	35.402500	688	667	633	92.0%			
6	217.416667	34.591389	574	572	566	98.6%			
7	217.441667	33.990833	551	546	529	96.0%			
8	217.454167	33.283889	865	861	839	97.0%			
9	218.245833	35.326667	652	631	602	92.3%			
10	218.133333	34.712222	728	720	686	94.2%			
11	218.225000	33.922500	614	612	603	98.2%			
12	218.395833	33.411389	785	766	749	95.4%			
13	219.020833	35.464167	786	717	697	88.7%			
14	218.895833	34.618056	748	664	636	88.8%			
15	219.091667	33.860833	855	737	711	83.2%			

Note. — These are the RA/Dec of the 15 standard sub-field centers, followed by the number of Main I-band (gcode06 = 524288) galaxies in the field, the number for which spectra were obtained, the number of successful redshift measurements and the resulting completeness. An object is in a field if it is closer to the center than  $R_{fld} = 0.49$  deg. Objects in overlapping fields are assigned to the closest field center, and objects in none of these standard sub-fields are given field number -1. See Fig. 2 for the positions of the fields on the sky.

 ${\bf Table\ 2.}\quad {\bf The\ Spectroscopic\ Observations}$ 

Pass	Field	Date	RA	Dec	$N_{exp}$	$T_{exp}$ (sec)	$N_{spec}$	Air Mass	Mean SNR	Comments
0	0	Spectra from the SDSS Survey					2946			
101	1	2004.0415	14:26:49.36	35:22:05.57	4	2400	268	1.03	16.21	
102	2	2004.0421	14:26:58.80	34:38:07.68	2	1800	266	1.01	11.21	
103	3	2004.0416	14:26:33.20	33:59:51.36	3	2700	263	1.02	16.51	
104	4	2004.0416	14:26:29.20	33:09:53.04	4	3600	267	1.19	14.92	major ADC
105	5	2004.0420	14:29:47.89	35:28:48.00	2	1440	262	1.12	7.09	
106	6	2004.0414	14:31:49.76	34:50:47.40	3	2700	267	1.18	7.66	not fluxed
107	7	2004.0420	14:29:41.89	33:53:09.36	2	1440	260	1.03	10.08	
108	8	2004.0422	14:29:37.09	33:13:53.04	2	1440	264	1.00	11.02	
109	9	2004.0420	14:32:38.18	35:23:05.99	2	1440	259	1.06	7.65	
110	10	2004.0414	14:31:49.76	34:50:47.40	3	2700	267	1.04	8.98	not fluxed
111	11	2004.0416	14:32:40.98	33:53:51.37	3	2700	263	1.02	18.17	
112	12	2004.0420	14:33:35.78	33:22:35.04	2	1440	268	1.01	10.06	
113	13	2004.0416	14:35:32.87	35:24:48.00	3	2700	258	1.20	14.22	major ADC
114	14	2004.0421	14:35:36.87	34:39:37.68	2	1440	270	1.01	8.53	
115	15	2004.0420	14:35:36.87	33:58:51.36	2	1440	270	1.09	9.74	
201	1	2004.0421	14:26:26.80	35:22:36.00	3	2700	259	1.09	9.00	
202	2	2004.0422	14:26:58.80	34:38:07.68	3	2700	258	1.07	8.00	
203	3	2004.0421	14:26:33.20	33:59:51.36	3	2700	259	1.28	9.03	major ADC
204	4	2004.0421	14:26:43.20	33:08:47.04	3	2700	268	1.04	8.87	
205	5	2004.0422	14:29:25.09	35:20:36.00	3	2700	244	1.29	6.94	major ADC
206	6	2004.0422	14:29:38.29	34:42:01.68	3	2700	262	1.10	10.89	
207	7	2004.0611	14:29:46.29	33:59:27.34	4	4500	264	1.08	10.21	
208	8	2004.0423	14:29:37.09	33:13:53.04	2	1800	264	1.32	5.60	major ADC
209	9	2004.0612	14:32:59.18	35:19:36.00	4	4500	276	1.08	10.87	not fluxed
210	10	2004.0422	14:32:39.38	34:40:49.68	3	2700	257	1.01	9.57	
211	11	2004.0423	14:32:42.98	33:54:21.36	3	2220	260	1.01	6.54	
212	12	2004.0423	14:33:35.78	33:22:35.04	3	2700	261	1.06	6.60	
213	13	2004.0420	14:35:45.27	35:28:48.00	3	2700	261	-1.00	9.34	major ADC
214	14	2004.0423	14:35:36.87	34:39:37.68	3	2700	254	1.11	5.74	
215	15	2004.0423	14:35:36.87	33:58:51.36	3	2700	259	1.01	7.20	

Table 2—Continued

Pass	Field	Date	RA	Dec	$N_{exp}$	$T_{exp}$ (sec)	$N_{spec}$	Air Mass	Mean SNR	Comments
301	1	2004.0610	14:27:00.40	35:21:54.01	4	4500	279	1.18	10.70	major ADC
302	2	2004.0620	14:26:40.40	34:34:43.68	4	4500	262	1.30	9.61	ADC off
303	3	2004.0622	14:27:04.00	33:50:18.36	4	4500	268	-1.00	10.93	
304	4	2004.0621	14:26:31.00	33:07:17.04	4	4500	264	1.37	9.68	major ADC
305	5	2004.0616	14:29:36.69	35:24:09.00	4	4500	272	1.06	9.33	
306	6	2004.0615	14:29:40.09	34:35:28.70	4	4500	265	1.06	12.24	
307	7	2004.0615	14:29:46.29	33:59:27.40	4	4500	263	1.30	9.53	major ADC
308	8	2004.0621	14:29:49.49	33:17:02.04	4	4500	272	1.07	10.92	
309	9	2004.0616	14:32:59.18	35:19:36.00	4	4500	268	1.29	9.45	major ADC
310	10	2004.0613	14:32:32.37	34:42:43.69	4	4500	265	1.04	11.61	not fluxed
311	11	2004.0614	14:32:53.97	33:55:21.36	4	4500	266	1.07	9.04	not fluxed
312	12	2004.0626	14:33:35.18	33:24:41.04	5	5625	260	1.03	6.59	scattered light
313	13	2004.0617	14:36:04.86	35:27:50.99	4	4500	266	-1.00	8.95	ADC off
314	14	2004.0618	14:35:34.87	34:37:04.68	4	4500	270	-1.00	10.94	ADC off
315	15	2004.0619	14:36:21.86	33:51:39.35	4	4500	267	1.15	10.96	ADC off
401	1	2005.0312	14:26:42.00	35:26:39.00	5	5400	261	1.05	9.12	
402	2	2005.0314	14:26:29.99	34:35:59.00	4	4080	241	1.03	3.82	
403	3	2005.0310	14:26:54.00	33:53:18.00	5	5100	261	1.04	11.17	
404	4	2005.0311	14:26:08.00	33:10:02.00	5	5400	253	1.04	18.58	
405	5	2005.0315	14:29:25.00	35:28:54.00	2	1800	253	1.03	3.09	
406	6	2005.0317	14:29:30.00	34:36:13.99	5	5400	250	1.05	13.39	
407	7	2005.0317	14:29:25.00	33:59:56.99	5	5400	249	1.33	5.49	
408	8	2005.0317	14:29:33.60	33:21:38.00	6	6480	247	1.04	11.42	
409	9	2005.0318	14:32:57.60	35:25:27.02	1	1080	244	1.00	6.38	
410	10	2005.0316	14:32:31.00	34:42:44.00	5	5400	253	1.04	10.37	
411	11	2005.0316	14:33:01.39	33:59:08.99	6	6480	246	1.04	10.27	
416	4	2005.0308	14:26:23.99	32:53:20.00	4	4320	260	1.03	15.12	
417	8	2005.0308	14:29:58.00	33:00:17.00	6	6480	261	1.08	18.75	
418	12	2005.0311	14:33:59.00	33:15:41.01	6	5400	259	1.30	11.45	
419	13	2005.0311	14:36:43.00	35:25:00.00	4	4320	258	1.04	13.25	
420	14	2005.0310	14:36:19.20	34:32:01.99	5	4800	253	1.03	14.06	

Table 2—Continued

Pass	Field	Date	RA	Dec	$N_{exp}$	$T_{exp}$ (sec)	$N_{spec}$	Air Mass	Mean SNR	Comments
421	15	2005.0312	14:36:52.20	33:54:17.99	5	5400	261	1.03	17.77	
422	1	2005.0309	14:27:06.00	35:23:23.90	5	5400	253	1.03	8.46	
423	4	2005.0314	14:26:20.99	33:07:01.90	5	5400	252	1.04	6.69	
501	1	2005.0406	14:26:48.34	35:25:45.65	5	4500	252	1.03	8.66	
502	2	2005.0406	14:26:39.39	34:34:54.39	3	3300	264	1.19	5.99	
503	3	2005.0409	14:26:38.90	33:43:36.41	4	3640	262	1.03	6.09	
504	4	2005.0408	14:26:22.44	33:07:01.47	5	5400	262	1.34	4.27	
505	5	2005.0409	14:30:35.16	35:30:22.56	4	4320	258	1.16	4.50	
506	6	2005.0407	14:30:46.60	34:51:20.84	5	5400	260	1.06	8.86	
507	7	2005.0410	14:30:18.65	34:00:55.58	4	4320	258	1.03	6.70	
508	8	2005.0410	14:30:46.73	33:12:25.94	5	4500	257	1.20	10.96	
510	10	2005.0411	14:32:07.71	34:40:38.06	5	5400	258	1.06	9.17	
511	11	2005.0411	14:33:05.26	34:00:44.66	4	4320	261	1.02	7.05	
512	12	2005.0411	14:33:33.74	33:23:28.63	4	4320	254	1.17	5.74	
522	1	2005.0405	14:26:19.24	35:12:59.23	3	3240	215	1.06	3.96	
523	2	2005.0405	14:26:28.60	34:35:57.20	3	3240	238	1.21	1.49	
524	3	2005.0406	14:26:49.00	33:49:38.72	3	3240	232	1.19	5.49	
525	7	2005.0407	14:29:12.19	34:16:33.70	2	1920	233	1.21	3.43	
526	2	2005.0406	14:26:49.79	34:48:52.29	4	4320	226	1.03	8.46	
601	1	2005.0506	14:26:46.00	35:26:22.00	5	5400	256	1.05	4.65	
602	2	2005.0507	14:26:32.00	34:36:44.00	6	6300	263	1.07	6.58	
603	3	2005.0510	14:26:50.00	33:53:03.00	4	4320	253	1.02	7.75	
604	4	2005.0510	14:26:22.00	33:07:01.99	2	2160	256	1.01	5.04	
605	5	2005.0509	14:29:25.00	35:28:54.00	5	5220	261	1.06	7.27	
606	6	2005.0508	14:29:30.00	34:36:13.98	6	6480	259	1.35	6.63	
607	7	2005.0509	14:29:25.00	33:59:56.99	5	5400	258	1.36	6.91	
608	8	2005.0510	14:29:57.60	33:16:10.01	4	4320	262	1.16	10.97	
609	9	2005.0512	14:32:57.59	35:25:27.02	5	5400	261	1.06	11.52	
610	10	2005.0510	14:32:31.00	34:42:44.00	3	3240	254	1.51	3.70	
611	11	2005.0511	14:33:01.39	33:59:08.99	4	4320	258	1.10	10.07	
612	12	2005.0514	14:33:55.00	33:22:44.99	5	5400	256	1.05	12.57	

Table 2—Continued

Pass	Field	Date	RA	Dec	$N_{exp}$	$T_{exp}$ (sec)	$N_{spec}$	Air Mass	Mean SNR	Comments
613	13	2005.0514	14:36:27.00	35:28:20.00	6	6480	261	1.37	14.64	
622	5	2005.0511	14:29:25.00	35:28:54.00	5	5400	258	1.47	5.85	
709	9	2005.0705	14:33:11.90	35:20:39.00	5	5400	257	1.23	7.34	
710	10	2005.0703	14:33:40.35	34:31:42.01	6	6480	259	1.09	3.76	
712	12	2005.0702	14:33:18.70	33:24:50.99	5	5400	260	1.05	9.78	
713	13	2005.0703	14:36:09.99	35:26:29.99	5	5400	258	1.50	8.96	
714	14	2005.0630	14:35:36.37	34:36:27.99	5	5400	258	1.12	8.22	
715	15	2005.0701	14:36:25.15	33:52:09.97	5	5400	258	1.08	13.82	
722	15	2005.0706	14:36:35.40	33:44:30.00	5	5400	241	1.14	11.81	
801	1	2006.0324	14:26:41.60	35:26:38.18	6	7200	256	1.12	7.34	
802	2	2006.0326	14:26:29.99	34:35:59.00	7	8400	263	1.14	8.07	
803	3	2006.0326	14:26:54.00	33:53:17.99	7	8400	265	1.09	10.16	
804	4	2006.0331	14:26:29.56	33:07:10.40	7	8400	266	1.07	8.08	
805	5	2006.0404	14:29:56.92	35:27:17.80	5	5107	261	1.04	6.08	
821	1	2006.0427	14:26:41.61	35:26:38.20	3	3600	252	1.14	5.18	
822	2	2006.0429	14:26:30.00	34:35:59.00	6	6600	260	1.33	7.69	
823	3	2006.0430	14:26:54.00	33:53:18.00	5	6000	267	1.04	9.01	
824	4	2006.0430	14:26:29.56	33:07:10.40	5	6000	261	1.29	10.56	
825	14	2006.0501	14:35:52.01	34:37:31.81	6	7200	263	1.34	6.04	
834	5	2006.0501	14:29:55.77	35:27:17.81	5	6000	262	1.04	9.77	
841	1	2006.0429	14:26:41.61	35:26:38.18	5	6000	251	1.04	7.88	
861			Coadded S	pectra			700		14.24	
862			Coadded S	pectra			700		13.66	
863			Coadded S	pectra			700		13.77	
906	6	2007.0510	14:29:15.42	34:37:34.98	5	9000	260	1.16	12.58	
908	13	2007.0219	14:36:24.00	35:27:05.00	3	5400	242	1.11	11.99	
909	9	2007.0513	14:32:58.13	35:25:27.02	5	9000	263	1.14	6.32	
910	10	2007.0512	14:32:49.54	34:45:25.01	6	10800	267	1.41	8.90	
911	11	2007.0513	14:32:21.67	33:54:24.01	6	10800	265	1.33	13.08	
912	12	2007.0315	14:33:56.00	33:20:45.00	6	10800	263	1.07	13.12	
914	14	2007.0615	14:35:54.43	34:37:10.99	3	5400	246	1.14	10.34	

1

Table 2—Continued

Pass	Field	Date	RA	Dec	$N_{exp}$	$T_{exp}$ (sec)	$N_{spec}$	Air Mass	Mean SNR	Comments
915	15	2007.0424	14:35:37.63	34:04:47.98	5	9000	262	1.18	11.72	
928	8	2007.0514	14:29:47.93	33:15:55.00	2	3600	264	1.02	10.02	
929	9	2007.0612	14:32:58.13	35:25:27.02	5	9000	252	1.39	7.38	
930	10	2007.0616	14:32:49.54	34:45:25.01	6	10800	264	1.23	5.62	
931	11	2007.0618	14:32:23.69	33:53:23.61	6	10800	263	1.19	11.80	
934	14	2007.0617	14:35:54.43	34:37:10.99	3	5400	263	1.02	12.72	
935	15	2007.0614	14:35:40.04	34:04:29.98	5	9000	252	1.27	10.93	
948	8	2007.0619	14:29:47.45	33:15:49.00	6	10800	261	1.18	15.23	
950	10	2007.0718	14:32:49.54	34:45:25.01	3	5400	264	1.30	4.77	

Note. — For each Pass we give the closest field center from Table 1, the RA/Dec of the pointing, the number of exposures, and the total exposure time.  $N_{spec}$  is the number of object spectra, Air Mass is the air mass near the middle of the exposures, Mean SNR is the mean signal-to-noise ratio of the object spectra.

Table 3. Final Samples In 2007

Sample Name	code06	Qshort/ Gshort	F/B/R	Total San	Main nple	Total Spe	Main ctra	Total Reds	Main shifts	Total Comple	Main eteness
WSRT	8	4		896	884	789	785	592	588	66%	67%
X-ray	16	8		3751	3282	3048	2895	2424	2294	65%	70%
MIPS	32	16		2347	2070	2125	1991	1843	1725	79%	83%
IRAC	64	32		5458	4759	4318	4079	3174	2977	58%	63%
MIPS	128	1	0.3/ 0.5 /30%	5284	4662	4588	4484	4510	4411	85%	95%
IRAC [8.0]	256	2	13.8/13.2/30%	4174	3536	3645	3498	3633	3490	87%	99%
IRAC [5.8]	512	4	15.2/14.7/30%	4771	4058	4173	3982	4110	3927	88%	98%
IRAC $[4.5]$	1024	8	15.7/15.2/30%	7261	6215	6324	6081	6234	5999	87%	98%
IRAC $[3.6]$	2048	16	15.7/15.2/30%	5861	4992	5095	4882	4999	4792	87%	98%
GALEX FUV	4096	32	22.0/22.5/30%	605	545	537	422	535	520	89%	96%
GALEX NUV	8192	64	22.0/21.0/30%	2068	1836	1838	1779	1832	1775	89%	97%
K-band	16384	128	16.5/16.0/20%	5676	5399	5431	5314	5416	5302	96%	98%
J-band	32768	256	18.5/17.5/20%	4517	4319	4288	4218	4278	4210	95%	98%
B-band	65536	512	21.3/20.5/20%	5097	4345	4471	4278	4426	4237	88%	99%
R-band	131072	1024	20.0/19.2/20%	8904	7480	7685	7378	7606	7304	86%	99%
Other I-band	262144	2048	20.0	22055	18368	8428	8257	7880	7727	36%	42%
Main I-band	524288	4096	20.0/18.5/20%	13122	11011	11019	10640	10667	10306	81%	94%

Note. — The Q/Gshort column gives the Qshort/Gshort code for the quasar (above rule) and galaxy (below rule) samples. For the galaxy samples, the F/B/R column gives the Faint limiting magnitude (or flux) of the sample, the Bright magnitude limit to which it is complete, and Random sampling fraction for the sources between the Bright and Faint magnitudes. For the  $24\mu m$  galaxy sample Bright/Faint are in mJy rather than magnitudes. The Total and Main columns give the number of targets overall and the number inside the 15 standard sub-fields. We list the size of each sample, the number for which spectra were obtained, the number of successful redshift measurements and the resulting completeness.

Table 4. Summary of AGN Selection

Sample	Case	Targs	Try	Fail	Succeed	Star	z > 0.5	> 1	> 2	> 3	> 4	Comment
WSRT	ALL	896	789	197	592	9	244	57	22	4	0	ALL
WSRT	pnt	132	123	28	95	8	63	41	18	3	0	point sources
WSRT	$\operatorname{gal}$	472	468	6	462	1	146	2	0	0	0	bright extended
WSRT	gal	292	198	163	35	0	35	14	4	1	0	faint, extended
X-ray	ALL	3751	3048	624	2424	135	1694	1084	325	57	3	ALL
X-ray	$\operatorname{pnt}$	1907	1685	191	1494	131	1263	983	302	50	3	point sources
X-ray	$\operatorname{gal}$	848	751	10	741	4	256	7	3	2	0	bright, extended
X-ray	gal	996	612	423	189	0	175	94	20	5	0	faint, extended
MIPS QSO	pnt	2347	2125	282	1843	41	1353	871	272	55	10	point sources
IRAC QSO	ALL	5458	4318	1144	3174	231	2071	1550	526	88	5	ALL
IRAC QSO	1	2887	2571	398	2173	207	1573	1294	405	62	3	point, bright red
IRAC QSO	2	405	291	133	158	5	129	113	74	13	1	point, faint, red
IRAC QSO	3	691	429	153	276	17	146	62	26	11	1	point, bright, bluer
IRAC QSO	4	237	118	2	216	0	61	4	1	0	0	extended, bright
IRAC QSO	5	759	447	357	90	1	88	70	19	1	0	extended, faint
ALL QSO		8977	7102	1885	5217	453	2926	1718	605	119	13	
ALL gals		35177	19447	900	18547	384	3341	12	6	3	0	

Note. — Quasar search yields for various samples, in some cases broken down into sub-categories.

Table 5. Summary of Selection Codes and Flags

RA	Dec	Code06	Code05	Code04	rcode	field	bstar	qirac	gal	qso	pntsrc	agngal
217.375476	32.806272	720896	720896	1536	0	8	0	0	1	0	0	1
217.893029	32.806415	724480	724480	2076	2	0	0	0	1	0	0	1
217.297011	32.806733	112	112	288	6	0	0	1	0	1	1	0
217.304623	32.806823	262144	262144	1024	6	0	0	0	1	0	0	1
216.311008	32.808259	589824	589824	1088	11	4	0	0	1	0	0	1
216.333753	32.806956	524288	524288	-1	16	4	0	0	1	0	0	1
216.393848	32.806964	724864	724864	2174	12	4	0	0	1	0	0	1
216.644254	32.806900	720896	720896	2112	10	4	0	0	1	0	0	1
217.088601	32.807106	262656	262784	-1	18	0	0	0	1	0	0	1
217.086404	32.807395	721152	721152	2112	11	0	0	0	1	0	0	1
217.479422	32.807504	524288	524288	-1	0	8	0	0	1	0	0	1
216.548230	32.807663	655360	655360	1536	3	4	0	0	1	0	0	1
217.228471	32.807886	262144	262144	-1	13	0	0	0	1	0	0	1
216.206669	32.808026	262144	262144	-1	10	4	0	0	1	0	0	1
216.199841	32.808199	16	-1	-1	5	4	0	0	0	1	0	1
216.845202	32.808131	262144	262144	1024	12	4	0	0	1	0	0	1
217.467032	32.808139	262272	262272	1024	12	8	0	0	1	0	0	1
216.328172	32.808479	0	0	-1	14	4	0	0	1	0	0	1
216.584225	32.808667	458752	458752	2112	10	4	0	0	1	0	0	1
217.618515	32.808876	524288	524288	-1	3	0	0	0	1	0	0	1

Note. — Code06, Code05, Code04 are the binary sample selection codes for the 2006/2007 (see §2.6), 2005 (see §2.5) and 2004 (see §2.4) survey periods, rcode is the random sample code, with each index representing a randomly selected 5% of the sources, field is the sub-field number, where 0 indicates that it is outside the standard fields. "qirac" gives the IRAC AGN selection sub-code for the 2006/2007 season. The codes gal, qso, pntsrc and agngal indicate whether the source was counted as a galaxy target, an AGN target, a point source, or a faint (I > 20 mag) extended AGN candidate. See §2 for a detailed definitions and discussions of the entries. The RA and Dec in this and later tables are the NDWFS DR3 I-band coordinates. The on-line version contains the complete table.

Table 6. Magnitudes And Fluxes

X	FUV	NUV	$\mathrm{B}_W$	R	I	z'	J	K1	K2	[3.6]	[4.5]	[5.8]	[8.0]	24
-10	-10.00	-10.00	20.71	19.29	18.77	19.13	-10.00	-10.00	-10.00	16.63	16.45	-10.00	14.02	-10.000
-10	-10.00	24.52	20.78	18.15	17.43	17.63	-10.00	-10.00	-10.00	14.53	14.46	14.40	14.27	-10.000
3	-10.00	-10.00	18.52	18.20	17.87	18.38	-10.00	-10.00	-10.00	14.66	13.72	12.85	11.81	3.474
-10	-10.00	-10.00	20.89	19.77	19.31	19.71	-10.00	-10.00	-10.00	17.44	17.51	-10.00	-10.00	-10.000
-10	-10.00	-10.00	20.43	19.71	17.27	19.77	-10.00	-10.00	-10.00	-10.00	16.81	-10.00	15.47	-10.000
-10	-10.00	-10.00	-10.00	20.94	18.22	21.51	-10.00	-10.00	-10.00	-10.00	-10.00	-10.00	-10.00	-10.000
-10	-10.00	-10.00	18.98	17.32	16.64	16.93	-10.00	-10.00	-10.00	14.00	13.94	13.29	10.82	2.775
-10	-10.00	-10.00	20.45	18.64	17.89	-10.00	-10.00	-10.00	-10.00	16.53	16.52	-10.00	14.93	-10.000
-10	-10.00	-10.00	22.25	20.01	19.15	19.29	-10.00	-10.00	-10.00	15.58	15.45	14.27	14.13	0.467
-10	-10.00	-10.00	20.29	18.59	17.95	18.14	-10.00	-10.00	-10.00	15.55	15.25	-10.00	12.94	-10.000
-10	-10.00	23.07	22.25	20.52	19.88	20.32	-10.00	-10.00	-10.00	17.18	16.51	-10.00	15.00	-10500
-10	-10.00	-10.00	22.08	19.92	19.21	19.38	-10.00	-10.00	-10.00	16.03	15.72	15.79	15.23	-10.000
-10	-10.00	-10.00	23.11	20.25	19.34	19.54	-10.00	-10.00	-10.00	16.14	16.05	16.14	-10.00	-10.000
-10	-10.00	-10.00	23.73	20.52	19.40	19.83	-10.00	-10.00	-10.00	-10.00	15.99	-10.00	15.74	-10.000
4	-10.00	-10.00	22.31	22.04	21.53	21.95	-10.00	-10.00	-10.00	-10.00	16.95	-10.00	15.44	-10.000
-10	-10.00	-10.00	21.50	19.65	18.98	19.35	-10.00	-10.00	-10.00	16.39	16.21	16.20	13.98	0.342
-10	-10.00	23.29	21.77	19.82	19.10	19.39	-10.00	-10.00	-10.00	15.87	15.46	15.15	13.67	0.693
-10	-10.00	-10.00	23.78	14.81	13.76	20.58	-10.00	-10.00	-10.00	13.68	13.39	-10.00	-10.00	-10.000
-10	-10.00	-10.00	20.36	19.15	18.67	19.07	-10.00	-10.00	-10.00	16.81	16.56	-10.00	14.24	-10.000
-10	-10.00	-10.00	23.09	20.57	19.79	19.84	-10.00	-10.00	-10.00	16.77	16.57	-10.00	14.78	-10.000

Note. — All entries except the X-ray column (X, counts) and  $24\mu$ m column (24, mJy) are in Vega magnitudes. An entry of -10 means no data or below the magnitude limit of the survey. X is from XBoötes (Murray et al. 2005, Kenter et al. 2005, Brand et al. 2006), FUV and NUV are from GALEX (Martin et al. 2005),  $B_W$ , R, I and K2 are from the NDWFS DR3 (Jannuzi & Dey 1999), z' is from zBoötes (Cool 2007), J and K1 are from FLAMEX (Elston et al. 2006), [3.6]-[8.0] are from the IRAC Shallow Survey (Eisenhardt et al. 2004) and the MIPS  $24\mu$ m fluxes are from Soifer & Spitzer/NOAO Team (2004). The on-line version contains the complete table.

Table 7. Redshifts

RA	Dec	N		Spectrur	n 1			Spectrur	n 2			Spectru	ım 3	
			z	S/N	pass	ap	z	S/N	pass	ap	z	S/N	pass	ap
217.375476	32.806272	1	0.219	9.009	308	230								
217.893029	32.806415	0												
217.297011	32.806733	1	1.257	34.483	108	100								
217.304623	32.806823	1	0.136	21.703	948	212								
216.311008	32.808259	2	0.352	2.745	604	100	-1.352	2.806	423	225				
216.333753	32.806956	0												
216.393848	32.806964	2	0.094	20.408	304	232	0.095	0.000	0	1				
216.644254	32.806900	1	0.131	3.534	204	90								
217.088601	32.807106	0												
217.086404	32.807395	1	0.132	15.873	304	177								
217.479422	32.807504	1	0.346	5.782	417	56								
216.548230	32.807663	1	0.248	9.615	304	213								
217.228471	32.807886	0												
216.206669	32.808026	1	0.534	2.297	604	102								
216.199841	32.808199	3	1.954	5.503	862	272	1.954	4.998	824	250	1.954	1.768	804	211
216.845202	32.808131	2	0.217	19.907	862	231	0.217	16.113	804	165				
217.467032	32.808139	1	0.346	9.655	608	181								
216.328172	32.808479	1	-4.218	3.240	404	199								
216.584225	32.808667	1	0.170	9.615	304	220								
217.618515	32.808876	0												

Note. — N indicates the number of spectra taken. The redshift z, signal-to-noise ratio S/N, pass and aperture codes (see §4) are then given for up to the first three spectra in order of decreasing S/N. Pipeline redshifts that did not pass visual inspection are reported as -1-z, where z was the pipeline redshift estimate. The on-line version contains the complete table.

Table 8. Photometric Redshifts

RA	Dec	$N_{band}$	$z_{phot}$	$\chi^2$	E Lu	Sbc minosity	$\frac{\mathrm{Im}}{L/10^{10}}$	$_{L_{\odot}}^{\mathrm{AGN}}$	E(B-V) mag
217.375476	32.806272	9	0.160	1.443	0.238	0.168	0.351	0.052	0.184
217.893029	32.806415	9	0.260	2.347	6.906	0.000	0.000	0.085	0.359
217.297011	32.806733	10	0.120	15.820	0.000	0.000	1.090	0.039	0.048
217.304623	32.806823	9	0.220	9.626	0.242	0.000	0.715	0.072	0.000
216.311008	32.808259	9	0.580	49.400	0.000	1.348	1.464	0.190	0.184
216.333753	32.806956	9	0.600	22.913	1.230	0.000	0.541	0.197	0.147
216.393848	32.806964	9	0.140	13.895	0.000	3.627	0.000	0.046	0.450
216.644254	32.806900	7	0.220	0.990	0.535	0.055	0.336	0.072	0.000
217.088601	32.807106	8	0.460	0.887	4.222	2.537	0.000	0.151	0.094
217.086404	32.807395	8	0.140	1.463	0.663	0.337	0.220	0.046	0.000
217.479422	32.807504	9	0.280	2.062	0.024	1.042	0.270	0.092	0.000
216.548230	32.807663	8	0.340	0.408	2.185	0.435	0.327	0.112	0.000
217.228471	32.807886	8	0.440	0.507	4.339	0.000	0.001	0.144	0.094
216.206669	32.808026	8	0.500	1.835	4.987	0.000	0.000	0.164	0.230
216.199841	32.808199	8	0.680	2.961	0.000	1.143	0.000	0.223	0.048
216.845202	32.808131	9	0.220	1.132	0.600	0.702	0.166	0.072	0.000
217.467032	32.808139	9	0.280	0.386	0.034	2.940	0.000	0.092	0.147
216.328172	32.808479	7	1.000	86.301	2.305	12.494	0.000	0.328	0.000
216.584225	32.808667	10	0.100	4.412	0.105	0.039	0.167	0.033	0.184
217.618515	32.808876	9	0.360	2.089	1.306	0.870	0.070	0.118	0.000

Note. — Photometric redshift and SED decompositions following Assef et al. (2010).  $N_{band}$  is the number of bands used to derive the photometric redshift  $z_{phot}$  and  $\chi^2$  is the goodness of fit at the photometric redshift. The E, Sbc, Im and AGN columns give the contributions of these templates to the SED in units of  $10^{10}L_{\odot}$ . By definition the contributions are always  $\geq 0$ , and they are calculated for the spectroscopic redshift if it is known. The AGN luminosity is only calculated redward of the Lyman limit. E(B-V) is the extinction applied to the AGN template. The on-line version contains the complete table.

Table 9. Spectra

Pass Aperture  $\lambda(\mathring{A})$  (Error)<sup>-1</sup> Spectrum Only in Electronic Version

Note. — The spectra as available. These are a mixture of results from the two pipelines and fluxed and un-fluxed spectra. Depending on the pipeline, the Error entry is either the inverse of the estimated noise in the spectrum or a masking flag. Fully homogenizing these reductions is beyond the scope of the present paper.

Table 10. Completeness and K-Corrections for the Galaxy Samples

RA	Dec	Completeness Corrections Spec Sparse Fiber		$z_{max}$	$V_{max}$	
		Spec	Sparse	Fiber		$10^6 h^{-3} \text{ Mpc}^3$
217.375476	32.806272	1.029	5.000	1.004	0.391	0.928
217.893029	32.806415					
217.297011	32.806733					
217.304623	32.806823					
216.311008	32.808259	1.054	1.000	1.004	2.346	47.569
216.333753	32.806956					
216.393848	32.806964	1.000	1.000	1.002	0.423	1.148
216.644254	32.806900	1.000	1.000	1.004	0.335	0.611
217.088601	32.807106					
217.086404	32.807395	1.000	1.000	1.000	0.335	0.609
217.479422	32.807504	1.040	5.000	1.307	0.364	0.768
216.548230	32.807663	1.003	5.000	1.004	0.355	0.719
217.228471	32.807886					
216.206669	32.808026	1.000	0.000	1.000	0.687	3.975
216.199841	32.808199					
216.845202	32.808131					
217.467032	32.808139	1.006	1.000	1.307	0.521	1.987
216.328172	32.808479					
216.584225	32.808667	1.006	1.000	1.002	0.322	0.547
217.618515	32.808876					

Note. — Factors needed to properly weight the galaxy samples following Cool et al. (2011). There are three completeness corrections factors. "Spec" corrects for the failure to determine a redshift when a spectrum was obtained, "Sparse" corrects for the target sparse sampling weighting, and "Fiber" corrects for how the local target density affects the assignment of fibers. The maximum redshift at which the source would have included the target is  $z_{max}$  and this corresponds to a volume of  $V_{max}$  in units of  $10^6h^{-3}$  Mpc<sup>3</sup> for an  $\Omega=0.3$ ,  $\Lambda=0.7$  cosmological model and the survey area of 7.60 deg<sup>2</sup> used by Cool et al. (2011). These are calculated using **kcorrect v4\_2** (Blanton & Roweis 2007) based on the  $B_w$ RI photometry.